Journal of Computational Physics 373 (2018) 673–697

Contents lists available at ScienceDirect

Journal of Computational Physics

www.elsevier.com/locate/jcp

Finite differences on staggered grids preserving the port-Hamiltonian structure with application to an acoustic duct ☆

Vincent Trenchant [a], Hector Ramirez [a], Yann Le Gorrec [a,*], Paul Kotyczka [b]

[a] FEMTO-ST Institute, AS2M department, Univ. Bourgogne Franche-Comté, Univ. de Franche-Comté/CNRS/ENSMM, 24 rue Savary, F-25000 Besançon, France

[b] Technical University of Munich, Department of Mechanical Engineering, Chair of Automatic Control, Boltzmannstraße 15, 85748 Garching, Germany

ARTICLE INFO

Article history:
Received 25 November 2017
Received in revised form 15 June 2018
Accepted 18 June 2018
Available online 30 June 2018

Keywords:
Distributed port-Hamiltonian systems
Wave equation
Staggered grids
Finite-difference method
Midpoint rule
Structured mesh

ABSTRACT

A finite-difference spatial discretization scheme that preserves the port-Hamiltonian structure of infinite dimensional systems governed by the wave equation is proposed. The scheme is based on the use of staggered grids for the discretization of different variables of the system. The discretization is given in 2D for rectilinear and regular triangular meshes. The proposed method is completed with the midpoint rule for time integration and numerical results are provided, including considerations for interconnection and closed loop behaviors and isotropy comparison between the proposed meshes.

1. Introduction

Discretization of distributed parameter systems is a key issue for simulation and control purposes. Among all existing and standard methods, the ones aiming at preserving structural invariants and structural properties of the original system are of particular interest when control design is considered. The aim of this paper is to revisit the standard finite-difference scheme in the light of port-Hamiltonian formulations to deal with the structural reduction of 1D and 2D systems driven by the wave equation. Port-Hamiltonian systems (PHS) stem from the representation of internal energy exchanges of multi-physical systems in interaction with their environment. They are particularly well suited to describe complex open systems interconnected through power conjugated port variables. The power preserving interconnection of subsystems is thereby formalized by the notion of Dirac structures [1,2], which represent a generalization of Kirchhoff's laws or Newton's laws and the velocity continuity in mechanics. For open systems, port-Hamiltonian systems cope with input and output flows and efforts [3]. By using this formalism, controlled systems can be interpreted in terms of the interconnection of physical systems exchanging energy among them, which from an engineering perspective provides a better understanding of the

☆ This work was supported by the Agence Nationale de la Recherche – Deutsche Forschungsgemeinschaft (ANR-DFG) project INFIDHEM, ID ANR-16-CE92-0028.

* Corresponding author.
E-mail addresses: vincent.trenchant@femto-st.fr (V. Trenchant), hector.ramirez@femto-st.fr (H. Ramirez), legorrec@femto-st.fr (Y. Le Gorrec), kotyczka@tum.de (P. Kotyczka).

https://doi.org/10.1016/j.jcp.2018.06.051
0021-9991/

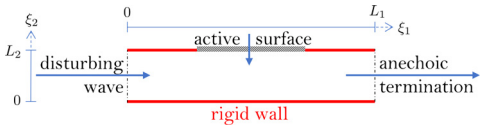

Fig. 1. Schematic representation of the physical system.

closed-loop system. This in turn permits to derive control strategies that are physically inspired [4]. Infinite-dimensional PHS governed by partial differential equations interconnected through their boundaries were introduced for modelling in [5,6] and extensions for control in for instance [7,2,8–10]. In the infinite-dimensional case, the Dirac structure underlying the PHS is expressed through differential operators. Performing a discretization which preserves the geometric structure of a PHS allows to preserve conservation laws and thus to preserve properties such as energy conservation and passivity with respect to the natural inputs and outputs of the system, which are central for control purposes. It also respects the physical meaning of the boundary port variables that can be naturally used for the interconnection of open multi-physical systems.

Several recent works tackle this challenge [11–15]. In [12,13], the structure of the system is preserved through the use of different (mixed) finite elements for the approximation of different variables. This approach found applications in modeling, reduction and control [16–19] and was extended through high order polynomial approximations to pseudo spectral approximations in [14]. In [20] a structure preserving finite-volume discretization for PHS was performed for the 1D case. The mixed Galerkin structure-preserving discretization for systems of conservation laws was presented recently in [21].

Finite differences is another important numerical method whose main advantage is its simplicity. It is based on the discretization of differential operators through Taylor series which lead to various schemes with different advantages such as convenience for particular geometries or convergence orders (see [22,23] for recent reviews). Among them, schemes presenting staggered grids [24–26] consider separately the state variables accordingly to their respective geometric nature. In [24], a generalized leapfrog structure is used in the time domain on the linear transport equation. It is shown that this method, if stable, preserves the conservation laws, which is an important property for the study of non-dissipative systems. Moreover, conditions for numerical stability are given therein. The proposed two steps methods apply only on closed systems and [20] can be considered as the extension to open systems from the finite volume point of view. For frequency domain modelling in 2D, the authors of [27–29] consider two staggered square grids, one of the grids being rotated. Changing the orientation of the grid allows to get high order approximations of the derivatives at the price of higher complexity, up to 25-point stencils. A simpler approach is proposed in [30] where finite differences are performed on simple staggered grids. The convenience of such a method for the wave propagation is illustrated on a seismologic example, where it allows to implement a velocity-stress formulation. Indeed, the use of staggered grids allows to impose the effort variables as boundary conditions, *e.g.* speed and pressure in acoustics, which is convenient for the study of open systems and interconnections, while a traditional finite-difference method would not. For the 2D and 3D cases, the meshing choice, for example the choice of rectilinear or triangular meshing, impacts the performance of the discretization. As mentioned in [31], if the use of rectangular grids leads straightforwardly to a good approximation of a considered PDE, a structured triangular mesh, also called hexagonal mesh [31,32], can at the cost of a higher complexity provide a better computational efficiency and is a better choice to emulate the isotropy of the spatial propagation of a wave. Indeed, a convenient choice of the discretization scheme through a compact structured mesh leads to a more homogeneous distribution of the propagation in space. In [33], schemes for a regular triangular mesh are proposed, including an explicit second-order method which leads to a simple and intuitive discretization of the first order differential operator, convenient for the discretization of the conservation laws underlying the wave equation. Another scheme, first proposed in [34] and used in [31], relies on a balanced propagation of the wave along the three axes of a regular triangular mesh for the second order differential operator of the wave equation.

Regarding time integration, since a staggered-grid method for PHS results in the approximation of first order time derivatives, explicit Euler, which is generally used in finite-difference time domain (FDTD) methods, is unconditionally unstable. Implicit midpoint, a symplectic method [35], is shown to be suited for non-dissipative PHS in [36]. Moreover, recent work [37] shows that there is a coincidence between the midpoint rule and discrete gradient in the linear case, which respects the power balance of the system.

In this paper, we propose to combine the port-Hamiltonian framework with finite differences on staggered grids to derive control oriented reduced order systems for the 2D wave equation. The differential operators which define the infinite-dimensional Stokes Dirac structure are approximated with a consistency of order 2 [38] by matrices which define a Dirac structure. In that sense, a finite-dimensional system derived from the proposed method is a PHS endowed in a Dirac structure which approximates the original Stokes Dirac structure. This work is motivated by the study of a generic acoustic control problem proposed in [39,40] and formulated as a port-Hamiltonian system in [41]. The considered system is an acoustic tube of rectangular section which is approximated using a 2D rectangular domain. Distributed actuation at the boundary (see Fig. 1) aims to dissipate part of the energy carried by the acoustic waves propagating inside the tube. Industrial applications can be found for example in aeronautics [42], air conditioning systems, motorised vehicles, etc., see [43] for a more exhaustive list. Even if the development of this work is motivated by this particular physical system, the discretization methods proposed in this paper apply to any linear 2D hyperbolic system.

The paper is organized as follows. In Section 2 the use of staggered grids for the spatial discretization through finite differences is motivated on the 1D wave equation. In Section 3 the 2D case is treated for a rectilinear and for a regular

triangular mesh. It is shown that the method preserves the port-Hamiltonian structure. In Section 4 numerical results are presented for the 1D and the 2D case for the rectilinear and the regular triangular meshes. The study is performed under open and closed loop conditions and the isotropy of the two meshes is compared. Finally in Section 5 we present general conclusions and comments of lines of future research. The notation used in this paper is recapitulated in the Appendix. A short recall on the considered time integration methods is given in a second appendix.

2. Distributed PHS and the 1D discretization scheme

In this section we introduce some basics on PHS and the use of the staggered-grid finite-difference method for PHS. We shall illustrate these concepts on the model of a 1D wave equation.

2.1. Distributed PHS

Consider the 1D wave equation

$$\frac{\partial^2 z}{\partial t^2}(\xi,t) = c_0^2 \frac{\partial^2 z}{\partial \xi^2}(\xi,t) \tag{1}$$

with $c_0 > 0 \in \mathbb{R}$ the celerity of the wave, $\xi \in [0, L]$, $L > 0 \in \mathbb{R}$ the space variable and $t \in \mathbb{R}^+$. To perform a discretization over the spatial domain, we define the spatial step $h > 0 \in \mathbb{R}$, and we consider a centered finite difference to approximate the first order spatial derivative at a point $\xi_k := kh$

$$\frac{\partial z}{\partial \xi}(\xi_k,t) \approx \frac{z_{k+0.5}(t) - z_{k-0.5}(t)}{h} \tag{2}$$

where $z_{k\pm0.5}(t) := z(\xi_k \pm 0.5h, t)$. The traditional finite-difference method allows to approximate the second order spatial derivative by applying again the approximation (2) on half-grid points $\xi_{k\pm0.5}$ leading to a scheme defined for every grid point k

$$\frac{\partial^2 z}{\partial t^2}(\xi_k,t) \approx c_0 \frac{z_{k+1}(t) - 2z_k(t) + z_{k-1}(t)}{h^2}. \tag{3}$$

It is known [44] that finite-difference schemes approximating derivatives of even order such as (3) induce numerical dissipation. To guarantee energy-preservation properties using spatial discretization, it is more convenient to consider the wave equation (1) as a set of first order balance equations. In the following we shall use as state variables

$$x_2 := -\frac{1}{q_1 q_2}\frac{\partial z}{\partial t}, \qquad x_1 := \frac{1}{q_1}\frac{\partial z}{\partial \xi},$$

with state vector $x = \begin{pmatrix} x_1 & x_2 \end{pmatrix}^\top$, and where $q_2 > 0 \in \mathbb{R}$ and $q_1 > 0 \in \mathbb{R}$ are physical parameters that depend on the considered physical domain. The balance equations underlying the wave equation are hence

$$\dot{x}_1 = -q_2 \frac{\partial x_2}{\partial \xi}, \qquad \dot{x}_2 = -q_1 \frac{\partial x_1}{\partial \xi},$$

such that $q_1 q_2 = c_0^2$.

On the physical example of a (linear) acoustic wave, z, x_1 and x_2 are respectively the velocity potential, the particular momentum and the opposite of the volume expansion. For this physical domain, $\frac{1}{q_1} = \mu_0$ is the mass density and $\frac{1}{q_2} = \chi_s$ is the adiabatic compressibility factor. In the following we keep this notation of the acoustic physical domain. However, all the following developments in this paper hold regardless of the physical domain considered.

Let us define a set of variables called flow and effort variables, respectively f_i and e_i, $i \in \{1, 2\}$, as

$$f = \begin{pmatrix} f_1 \\ f_2 \end{pmatrix} = \begin{pmatrix} \dot{x}_1 \\ \dot{x}_2 \end{pmatrix}, \qquad e = \begin{pmatrix} e_1 \\ e_2 \end{pmatrix} = \mathcal{L}\begin{pmatrix} x_1 \\ x_2 \end{pmatrix} \tag{4}$$

with $\mathcal{L} = \begin{pmatrix} \mu_0^{-1} & 0 \\ 0 & \chi_s^{-1} \end{pmatrix}$. The vectors f and e are called the vector of flows and the vector of efforts, respectively. In the acoustic framework, e_1 and e_2 correspond to the particular speed and to the acoustic pressure, respectively. There is a linear relation between the flow and effort vectors given by

$$f = \mathcal{J} e, \qquad \text{with} \qquad \mathcal{J} = \begin{pmatrix} 0 & -\frac{\partial}{\partial \xi} \\ -\frac{\partial}{\partial \xi} & 0 \end{pmatrix}. \tag{5}$$

When this relation is completed with the definition of the total energy of the system, which is given by a functional $\mathcal{H}$ defined by

$$\mathcal{H}(x) = \frac{1}{2}\int_0^L x^\top \mathcal{L} x \, d\xi \tag{6}$$

for any smooth real function $x(\xi, t)$ where the integrand in the integral form of $\mathcal{H}$ is a smooth function of x, and a set of boundary conditions, then (5) defines a distributed port-Hamiltonian system [5,2]. The total energy of the system (6) is called the Hamiltonian and the state variables are called energy variables. The boundary conditions, which correspond to the evaluation at the spatial boundaries of the effort vector e, are given by

$$\begin{pmatrix} f_\partial \\ e_\partial \end{pmatrix} := U \begin{pmatrix} e_1(0) \\ -e_2(L) \\ e_2(0) \\ e_1(L) \end{pmatrix} \tag{7}$$

U is a unitary transformation that does not modify the energy balance *i.e.* the product $f_\partial^T e_\partial$ and allows to characterize all the possible boundary port variables that respect this balance. In [5,6], it is shown that $\mathcal{J}$ is formally skew-symmetric with respect to the set of boundary variables (7). All possible parameterizations of (7) can be found in [6,8]. Geometrically a PHS is endowed in a Dirac structure [1], which defines a formal linear relation between flows and efforts. Physically, a Dirac structure is the geometrical expression of power preserving interconnection laws, such as Kirchhoff's and Newton's laws. In the case of distributed PHS with non zero boundary conditions the definition of the Dirac structure is extended in order to cope with the power flowing through the boundaries. This class of structure is called a Stokes–Dirac structure [5]. We do not give the definition of a Stokes–Dirac structure in infinite dimension, which can be found in [5], since it requires to introduce notions of differential geometry which are not relevant to the developments of the paper. The discrete systems which stem from the structure preserving discretization method we propose define Dirac structures in finite dimension. However, since the objective is to obtain a finite-dimensional PHS, we define the Dirac structure in finite dimensions.

Definition 1. [1] In finite dimensions a Dirac structure $\mathcal{D}_d$ is a subspace of $\mathcal{F} \times \mathcal{E}$ where $\mathcal{F}$ is a linear space and $\mathcal{E}$ its dual space, such that $\mathcal{D}_d = \mathcal{D}_d^\perp$ with respect to the symmetrical bilinear form

$$\langle (f_d^1, e_d^1) | (f_d^2, e_d^2) \rangle = \langle e_d^1, f_d^2 \rangle + \langle e_d^2, f_d^1 \rangle \tag{8}$$

for $(f_d^i, e_d^i) \in \mathcal{F} \times \mathcal{E}$, $i \in \{1, 2\}$ and $\langle \cdot, \cdot \rangle_d$ the canonical product on $\mathcal{F} \times \mathcal{E}$ such that $\langle f_d, e_d \rangle = f_d^\top e_d$.

The Dirac structure is a linear algebraic relation between flows and efforts. In order to obtain an explicit representation, state variables and causality relations have to be assigned.

Definition 2. [1] A port-Hamiltonian system without internal dissipation is defined by a Dirac structure $\mathcal{D}_d$ and a Hamiltonian $H\colon \mathcal{X} \to \mathbb{R}$ where $\mathcal{X}$ contains the vectors of energy variables x. The dynamics is given by the requirement that

$$\left(f, e, f_p, e_p\right) \in \mathcal{D}_d$$

where $f = \dot{x}$, $e = \frac{\partial H(x)}{\partial x}$, and where f_p and e_p are the flows and efforts of the external ports *i.e.* the exchanges between the system and its environment.

This definition also applies for infinite-dimensional systems [5,6] when the effort e is chosen equal to the variational derivative $\frac{\delta H(x)}{\delta x}$ and when f_p and e_p correspond to the boundary flow and effort vectors.

Remark 3. In the 1D case [45] the variational derivative of a functional $\mathcal{H}$ of the form

$$\mathcal{H}(x) = \frac{1}{2}\int_\Omega x(\xi)^\top \mathcal{L}(\xi) x(\xi) d\xi$$

with $\mathcal{L} \in L^\infty\left([0, L]; \mathbb{R}^{n \times n}\right)$ such that $\mathcal{L}^* = \mathcal{L}$, $mI \leq \mathcal{L}(\xi) \leq MI$ for $\xi \in [0, L]$ and constants $m, M > 0$ is given by

$$\frac{\delta \mathcal{H}}{\delta x}(x) = \mathcal{L} x.$$

In the case of the wave equation, since $\mathcal{J}$ is formally skew-symmetric with respect to f_∂, e_∂, and since $e = \mathcal{L}x = \frac{\delta \mathcal{H}}{\delta x}$, the system (5), (7) defines an infinite-dimensional port-Hamiltonian system. It is not difficult to verify that the energy balance is given in terms of the boundary variables [5]

$$\dot{\mathcal{H}} = f_\partial^\top e_\partial = e_1(0)e_2(0) - e_2(L)e_1(L). \tag{9}$$

In the following section we shall proceed to discretize this class of systems.

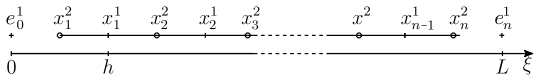

Fig. 2. 1D staggered discretization of x_d^1, x_d^2.

2.2. 1D spatial discretization

In this subsection we perform the spatial discretization of the wave equation (1) from its port-Hamiltonian formulation (4)–(7) where (5) can be explicitly written

$$\begin{pmatrix} \dot{x}_1 \\ \dot{x}_2 \end{pmatrix} = \begin{pmatrix} 0 & -\frac{\partial}{\partial \xi} \\ -\frac{\partial}{\partial \xi} & 0 \end{pmatrix} \begin{pmatrix} \frac{1}{\mu_0} & 0 \\ 0 & \frac{1}{\chi_s} \end{pmatrix} \begin{pmatrix} x_1 \\ x_2 \end{pmatrix}$$

with $x_1(\xi,0) = x_{1,0}$ and $x_2(\xi,0) = x_{2,0}$ and $e_1(0,t) = u_1(t)$ and $e_1(L,t) = u_2(t)$. In the acoustic framework, this is equivalent to imposing the particular velocity at the boundary, which corresponds to Neumann conditions regarding the second order wave equation in z (1). The spatial discretization, also known as semi-discretization, is performed according to boundary conditions whose natures are chosen a priori and which are imposed at the boundary points. For the sake of simplicity we shall consider a constant spatial step $h \in \mathbb{R} > 0$ such that one can find a $n \in \mathbb{N}$ with $nh = L$. The state of the system (5), (7) is discretized over the grids described in Fig. 2, the boundary conditions are thus conditions over $e_1(0,t)$ and $e_1(L,t)$ which can be interpreted as inputs of the system. Their discrete counterparts are denoted by e_0^1 and e_n^1, respectively.

Remark 4. The causality, i.e. the nature of the boundary conditions, has to be chosen a priori since it is critical for the definition of the different staggered grids and for the numbering of the discrete variables. Even if the proposed method is presented in this section through one example of causality, it can be applied on any configuration of boundary conditions without further difficulties. For example, another set of boundary conditions is considered in [38] where the pressure e_2 is imposed at one of the boundaries. Imposing e_2 at the boundary corresponds to a Dirichlet condition regarding a second order wave equation in pressure $\frac{\partial^2 e_2(\xi,t)}{\partial t^2} = c_0^2 \frac{\partial^2 e_2(\xi,t)}{\partial \xi^2}$. The possibility to impose directly the particular speed e_1 and the pressure e_2 at different boundaries of the same system comes as an advantage of the use of staggered grids over traditional discretization methods such as finite elements. See also [15] for different boundary causalities from the perspective of discrete modeling of conservation laws.

To perform the semi-discretization, the state variables are approximated by the finite-dimensional vector $x_d = \left((x_d^1)^\top \quad (x_d^2)^\top\right)^\top \in \mathbb{R}^{2n-1}$ with $x_d^1 = \begin{pmatrix} x_1^1 & \dots & x_{n-1}^1 \end{pmatrix}^\top$ the vector of elements evaluated on the integer points of discretization, $\xi_k = kh$, $k \in \{0 \dots n\}$ and $x_d^2 = \begin{pmatrix} x_1^2 & \dots & x_n^2 \end{pmatrix}^\top$ the vector of elements evaluated on the half-integer points, $\xi_k = (k+0.5)h$, $k \in \{1 \dots n\}$. A discrete Hamiltonian H_d is defined as

$$H_d := \frac{1}{2} x_d^\top L_d x_d = \frac{1}{2} \left(\frac{1}{\chi_s} (x_n^2)^2 + \sum_{i=1}^{n-1} \begin{pmatrix} x_i^1 & x_i^2 \end{pmatrix} \begin{pmatrix} \mu_0^{-1} & 0 \\ 0 & \chi_s^{-1} \end{pmatrix} \begin{pmatrix} x_i^1 \\ x_i^2 \end{pmatrix} \right) \tag{10}$$

where $L_d \in \mathbb{R}^{(2n-1)\times(2n-1)}$ is a diagonal matrix which corresponds to $\mathcal{L}$ evaluated at the corresponding grid points. Note that $hH_d \approx \mathcal{H}(x)$ in the sense that hH_d converges to $\mathcal{H}(x)$ when n tends to infinity. The vector of discrete efforts is derived from (10)

$$e_d := \frac{\partial H_d}{\partial x_d} = L_d x_d \tag{11}$$

where $e_d = \left((e_d^1)^\top \quad (e_d^2)^\top\right)^\top \in \mathbb{R}^{2n-1}$ with $e_d^1 = \begin{pmatrix} e_1^1 & \dots & e_{n-1}^1 \end{pmatrix}^\top$ and $e_d^2 = \begin{pmatrix} e_1^2 & \dots & e_n^2 \end{pmatrix}^\top$. The central finite difference scheme (2) can then be applied to obtain

$$\begin{aligned} \frac{\partial e_1}{\partial \xi}(\xi_k, t) &\approx \frac{e_1(\xi_{k+0.5}, t) - e_1(\xi_{k-0.5}, t)}{h} = \frac{e_k^1 - e_{k-1}^1}{h}, \\ \frac{\partial e_2}{\partial \xi}(\xi_{k+0.5}, t) &\approx \frac{e_2(\xi_{k+1}, t) - e_2(\xi_k, t)}{h} = \frac{e_{k+1}^2 - e_k^2}{h}. \end{aligned} \tag{12}$$

One expresses f_d, a discrete approximation of the flow $f = \mathcal{J}e$, as $f_d = \begin{pmatrix} f_d^1 & f_d^2 \end{pmatrix}^\top = \begin{pmatrix} f_1^1 & \dots & f_{n-1}^1 & f_1^2 & \dots & f_n^2 \end{pmatrix}^\top$ with

$$f_d^1 = \underbrace{-\frac{1}{h}\begin{pmatrix} -1 & 1 & & \\ & \ddots & \ddots & \\ & & -1 & 1 \end{pmatrix}}_{D\in\mathbb{R}^{(n-1)\times n}} e_d^2, \qquad f_d^2 = \underbrace{-\frac{1}{h}\begin{pmatrix} 1 & & \\ -1 & \ddots & \\ & \ddots & 1 \\ & & -1 \end{pmatrix}}_{-D^\top\in\mathbb{R}^{n\times(n-1)}} e_d^1 + \frac{1}{h}\begin{pmatrix} 1 & 0 \\ 0 & 0 \\ \vdots & \vdots \\ 0 & -1 \end{pmatrix}\begin{pmatrix} e_0^1 \\ e_n^1 \end{pmatrix}. \tag{13}$$

The complete discrete flow vector is then

$$f_d = \underbrace{\begin{pmatrix} 0 & D \\ -D^\top & 0 \end{pmatrix}}_{J_d} e_d + \underbrace{\frac{1}{h}\begin{pmatrix} 0_{n,2} \\ \begin{matrix} 1 & 0 \\ 0 & 0 \\ \vdots & \vdots \\ 0 & -1 \end{matrix} \end{pmatrix}}_{g_d}\begin{pmatrix} e_0^1 \\ e_n^1 \end{pmatrix} \tag{14}$$

where J_d is skew-symmetric.[1]

Proposition 5. *The staggered-grid finite-difference spatial discretization of (5) according to the scheme (12) defines a finite-dimensional Dirac structure $\mathcal{D}_d$ which approximates the original Stokes–Dirac structure. The approximated system*

$$\begin{cases} \dot{x}_d = J_d L_d x_d + g_d u_d \\ y_d = g_d^\top e_d \end{cases} \tag{15}$$

with $u_d = e_d^\partial = \begin{pmatrix} e_0^1 \\ e_n^1 \end{pmatrix}$ and $y_d = f_d^\partial = \begin{pmatrix} \frac{1}{h}e_1^2 \\ -\frac{1}{h}e_n^2 \end{pmatrix}$, is thus a PHS.

Proof. Define $e'_d = \begin{pmatrix} e_d \\ e_d^\partial \end{pmatrix} \in \mathbb{R}^{2n+1} =: E$, $f'_d = \begin{pmatrix} f_d \\ -f_d^\partial \end{pmatrix} \in \mathbb{R}^{2n+1} =: F$ and $J' = \begin{pmatrix} J_d & g_d \\ -g_d^\top & 0 \end{pmatrix} = -J'^\top$ such that $f'_d = J'e'_d$. $\mathcal{D}_d \subset F \times E$ is a Dirac structure if and only if $\mathcal{D}_d = \mathcal{D}_d^\perp$ with $\mathcal{D}_d^\perp = \{(f_a, e_a) \in F \times E | \langle (f_a, e_a) | (f_b, e_b) \rangle = 0 \ \forall (f_b, e_b) \in \mathcal{D}_d\}$. For all (f'_a, e'_a) and (f'_b, e'_b) in $\mathcal{D}_d$,

$$\begin{aligned} \langle (f'_a, e'_a) | (f'_b, e'_b) \rangle &= \langle e'_a, f'_b \rangle + \langle e'_b, f'_a \rangle \\ &= \langle e'_a, J'e'_b \rangle + \langle e'_b, J'e'_a \rangle \\ &= \langle e'_a, J'e'_b \rangle - \langle e'_a, J'e'_b \rangle \\ &= 0 \Leftrightarrow (f'_a, e'_a) \in \mathcal{D}_d^\perp \Leftrightarrow \mathcal{D}_d \subset \mathcal{D}_d^\top. \end{aligned}$$

Consider now $(f'_a, e'_a) \in \mathcal{D}_d^\perp$ and $(f'_b, e'_b) \in \mathcal{D}_d$.

$$\begin{aligned} \langle (f'_a, e'_a) | (f'_b, e'_b) \rangle &= 0 \\ &= \langle e'_a, f'_b \rangle + \langle e'_b, f'_a \rangle \\ &= \langle e'_a, J'e'_b \rangle + \langle e'_b, f'_a \rangle \\ &= -\langle e'_b, J'e'_a \rangle + \langle e'_b, f'_a \rangle. \end{aligned}$$

Since this equality is true for all $(f'_b, e'_b) \in \mathcal{D}_d$, then $f'_a = J'e'_a$ and then $\mathcal{D}_d^\top \subset \mathcal{D}_d$. $\mathcal{D}_d$ is then a Dirac structure. □

Remark 6. The energy balance of the PHS (15) is

$$\begin{aligned} \dot{H}_d(t) &= \frac{1}{h}(e_0^1 e_1^2 - e_n^1 e_n^2) \\ &\approx \frac{1}{h}\left(e^1(0,t)e^2(0.5h,t) - e^1(L-0.5h,t)e^2(L,t)\right) \end{aligned} \tag{16}$$

and $h\dot{H}_d(t)$ tends to $\dot{\mathcal{H}}(t) = f_\partial^\top(t)e_\partial(t)$ when $h \to 0$.

[1] $0_{n,m}$ is the $n \times m$ null matrix and 0 represents the null matrices of appropriate dimensions when there is no ambiguity.

Remark 7. It can be shown [38], at least numerically, that the spectrum of the approximated model tends to the infinite dimensional one when h tends to zero. In Section 4 of [19], this property is shown theoretically in the framework of mixed finite elements by considering the spectrum of a discretization matrix which coincides with J_d. However, the extension of this result to our discretization method needs particular care and is kept for future work.

3. Discretization of the 2D wave equation

The extension of finite difference on staggered grids to 2D systems allows to approximate the wave equation while preserving its inner structural properties related to conservation laws such as the conservation of energy, and guarantees the physical meaning of the boundary variables. Since the main interest in using the finite-difference method is its simplicity, only cases with structured meshes (rectilinear and regular triangular grids) are considered in this work. In the next subsections we first present the PHS formulation of 2D the wave equation and then propose structure preserving discretization schemes on rectilinear and triangular grids.

3.1. The PHS formulation of the system

Consider a rectangular domain Ω with orthonormal coordinates $\xi_1 \in [0, L_1]$, $\xi_2 \in [0, L_2]$. Consider as state vector[2] $x = \begin{pmatrix} x_1 \\ x_2 \\ x_3 \end{pmatrix} \in L_2(\Omega, \mathbb{R}^3) = \mathcal{X}$ and the balance equations

$$\begin{pmatrix} \dot{x}_1 \\ \dot{x}_2 \end{pmatrix} = -\begin{pmatrix} \frac{\partial}{\partial \xi_1} \\ \frac{\partial}{\partial \xi_2} \end{pmatrix} (\chi_s^{-1} x_3), \qquad \dot{x}_3 = -\begin{pmatrix} \frac{\partial}{\partial \xi_1} & \frac{\partial}{\partial \xi_2} \end{pmatrix} \begin{pmatrix} \mu_0^{-1} x_1 \\ \mu_0^{-1} x_2 \end{pmatrix}, \tag{17}$$

where the operators $\begin{pmatrix} \frac{\partial}{\partial \xi_1} \\ \frac{\partial}{\partial \xi_2} \end{pmatrix}$ and $\begin{pmatrix} \frac{\partial}{\partial \xi_1} & \frac{\partial}{\partial \xi_2} \end{pmatrix}$ are the gradient and divergence, respectively.

In the general case where μ_0 and χ_s are dependent on space, these balance equations lead to the non-uniform wave equation

$$\chi_s \ddot{z} = div\left(\frac{1}{\mu_0} grad(z)\right) \tag{18}$$

where z is defined such that $grad(z) = x_1$.

Assume that the balance equations (17) represent a physical system with kinetic energy E_k and potential energy E_p defined as

$$\begin{aligned} E_k &= \frac{1}{2} \int_0^{L_1} \int_0^{L_2} \begin{pmatrix} x_1 & x_2 \end{pmatrix} \frac{1}{\mu_0} \begin{pmatrix} x_1 \\ x_2 \end{pmatrix} d\xi_2 d\xi_1 \\ E_p &= \frac{1}{2} \int_0^{L_1} \int_0^{L_2} x_3 \frac{1}{\chi_s} x_3 \, d\xi_2 d\xi_1. \end{aligned} \tag{19}$$

In the case of an acoustic system, $\begin{pmatrix} x_1 \\ x_2 \end{pmatrix}$ and x_3 may be interpreted as density of momentum and as the opposite of the volume expansion coefficient, respectively [41]. In this framework, the two balance equations (17) stem from mass conservation and Newton's third law, respectively. The Hamiltonian $\mathcal{H} : \mathcal{X} \to \mathbb{R}$ of the system corresponds to its total energy, *i.e.* the sum of E_k and E_p, such that

$$\mathcal{H}(x) = \frac{1}{2} \int_0^{L_1} \int_0^{L_2} x^\top \mathcal{L} x \, d\xi_2 d\xi_1 \tag{20}$$

with $\mathcal{L} = \begin{pmatrix} \mu_0^{-1} & 0 & 0 \\ 0 & \mu_0^{-1} & 0 \\ 0 & 0 & \chi_s^{-1} \end{pmatrix}$. The flow variables f_i and the effort variables e_i, $i \in \{1, 2, 3\}$, are defined along with the vector of flows f and the vector of efforts e,

$$f = \begin{pmatrix} f_1 \\ f_2 \\ f_3 \end{pmatrix} = \begin{pmatrix} \dot{x}_1 \\ \dot{x}_2 \\ \dot{x}_3 \end{pmatrix}, \qquad e = \begin{pmatrix} e_1 \\ e_2 \\ e_3 \end{pmatrix} = \frac{\delta \mathcal{H}}{\delta x} = \mathcal{L} \begin{pmatrix} x_1 \\ x_2 \\ x_3 \end{pmatrix}.$$

[2] $L^2(\Omega, \mathbb{R}^n)$ denotes the space of square-integrable functions on the domain Ω with vector values in $\mathbb{R}^n$.

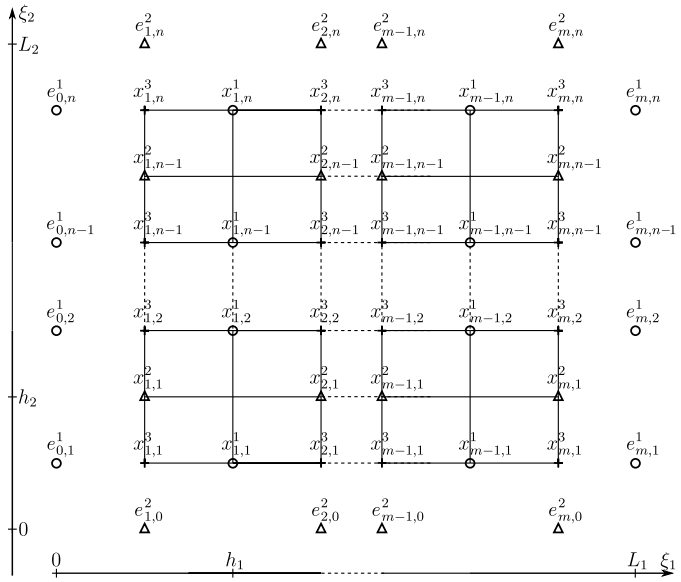

Fig. 3. 2D discretization grid.

In the acoustic framework, the effort variables $\begin{pmatrix} e_1 \\ e_2 \end{pmatrix}$ and e_3 represent the particular speed and the pressure, respectively. The linear relation between flow and effort vectors is then expressed from the balance equations (17) as a combination of the gradient and divergence operators such that

$$f = \mathcal{J} e, \qquad \text{with} \qquad \mathcal{J} = \begin{pmatrix} 0 & 0 & -\frac{\partial}{\partial \xi_1} \\ 0 & 0 & -\frac{\partial}{\partial \xi_2} \\ -\frac{\partial}{\partial \xi_1} & -\frac{\partial}{\partial \xi_2} & 0 \end{pmatrix}, \tag{21}$$

and can be written explicitly

$$\begin{pmatrix} \dot{x}_1 \\ \dot{x}_2 \\ \dot{x}_3 \end{pmatrix} = \begin{pmatrix} 0 & 0 & -\frac{\partial}{\partial \xi_1} \\ 0 & 0 & -\frac{\partial}{\partial \xi_2} \\ -\frac{\partial}{\partial \xi_1} & -\frac{\partial}{\partial \xi_2} & 0 \end{pmatrix} \begin{pmatrix} \mu_0^{-1} & 0 & 0 \\ 0 & \mu_0^{-1} & 0 \\ 0 & 0 & \chi_s^{-1} \end{pmatrix} \begin{pmatrix} x_1 \\ x_2 \\ x_3 \end{pmatrix}. \tag{22}$$

This relation defines a port-Hamiltonian system [41] for the Hamiltonian (20) and for the set of boundary conditions

$$\begin{pmatrix} f_\partial \\ e_\partial \end{pmatrix} = \begin{pmatrix} f_{\partial 1} \\ f_{\partial 2} \\ e_{\partial 1} \\ e_{\partial 2} \end{pmatrix} = U \begin{pmatrix} -e_3(L_1,\xi_2) \\ e_3(0,\xi_2) \\ -e_3(\xi_1,L_2) \\ e_3(\xi_1,0) \\ e_1(L_1,\xi_2) \\ e_1(0,\xi_2) \\ e_2(\xi_1,L_2) \\ e_2(\xi_1,0) \end{pmatrix} \tag{23}$$

with U a unitary transformation and where $f_{\partial i}$ and $e_{\partial i}$, $i \in \{1,2\}$ are in $\mathbb{R}^2$. The energy balance satisfies [41]

$$\frac{dH}{dt} = \int_0^{L_1} f_{\partial 2}^\top e_{\partial 2} d\xi_1 + \int_0^{L_2} f_{\partial 1}^\top e_{\partial 1} d\xi_2 \tag{24}$$

where the right-hand side corresponds to the expression in coordinates of $\int_{\mathcal{B}} f_\partial^\top e_\partial ds$, *i.e.* the integral on the boundary of the domain $\mathcal{B}$. This means that the variation of the total energy of the system corresponds to the power exchange with its environment through the boundaries. We consider the discretization of this system with initial conditions $x_1(\xi_1,\xi_2,0) = x_{1,0}$, $x_2(\xi_1,\xi_2,0) = x_{2,0}$ and $x_3(\xi_1,\xi_2,0) = x_{3,0}$ and with boundary conditions imposing $e_1(L_1,\xi_2) = u_1(t)$, $e_1(0,\xi_2) = u_2(t)$, $e_2(\xi_1,L_2) = u_3(t)$ and $e_2(\xi_1,0) = u_4(t)$ as inputs of the system. These boundary conditions correspond to impose U equals to identity in (23).

3.2. Rectilinear grids

Defining h_1, respectively h_2, the spatial step along ξ_1 respectively ξ_2), the states of the system (22), (23) are discretized over the grids described in Fig. 3. The boundary conditions are given by the efforts imposed on boundary

points numbered $(0, k_2)$ and (m, k_2) for conditions on e_1 and $(k_1, 0)$ and (k_1, n) for conditions on e_2, with $k_2 \in \{1...n\}$ and $k_1 \in \{1...m\}$. This corresponds in the acoustic framework to impose at each boundary the normal component of the particular speed. In the discretized setting, the continuous state variables are replaced by the finite-dimensional vector $x_d = \left((x_d^1)^\top \quad (x_d^2)^\top \quad (x_d^3)^\top\right)^\top \in \mathbb{R}^{3mn-(m+n)}$, with

$$\begin{aligned} x_d^1 &= \begin{pmatrix} x_{1,1}^1 & x_{1,2}^1 & \cdots & x_{m-1,n}^1 \end{pmatrix}^\top \in \mathbb{R}^{(m-1)n}, \\ x_d^2 &= \begin{pmatrix} x_{1,1}^2 & x_{1,2}^2 & \cdots & x_{m,n-1}^2 \end{pmatrix}^\top \in \mathbb{R}^{m(n-1)}, \\ x_d^3 &= \begin{pmatrix} x_{1,1}^3 & x_{1,2}^3 & \cdots & x_{m,n}^3 \end{pmatrix}^\top \in \mathbb{R}^{mn}, \end{aligned} \tag{25}$$

and the boundary effort variables by the finite-dimensional vector $e_d^\partial = \left((e_{d\partial}^1)^\top \quad (e_{d\partial}^2)^\top \quad (e_{d\partial}^3)^\top\right)^\top$, with

$$\begin{aligned} e_{d\partial}^1 &= \begin{pmatrix} e_{0,1}^1 & e_{0,2}^1 & \cdots & e_{0,n}^1 & e_{m,1}^1 & e_{m,2}^1 & .. & e_{m,n}^1 \end{pmatrix}^\top, \\ e_{d\partial}^2 &= \begin{pmatrix} e_{1,0}^2 & e_{1,n}^2 & e_{2,0}^2 & e_{2,n}^2 & \cdots & e_{m,0}^2 & e_{m,n}^2 \end{pmatrix}^\top. \end{aligned} \tag{26}$$

$e_{d\partial}^3$ is equal to the empty set in this particular case due to the choice of boundary conditions which are on e_1 or e_2 along the boundary. The discrete Hamiltonian H_d is defined in terms of the discretized states x_d as

$$H_d := \tfrac{1}{2} x_d^\top L_d x_d \tag{27}$$

where $L_d \in \mathbb{R}^{(3mn-(m+n))\times(3mn-(m+n))}$ is a diagonal matrix which corresponds to $\mathcal{L}$ evaluated at the corresponding grid points. Note that $h_1 h_2 H_d \approx H$ in the sense that $h_1 h_2 H_d$ converges to H when m and n tend to infinity. Defining the vector of discrete efforts as the gradient of the discrete energy,

$$e_d := \left(\frac{\partial H_d}{\partial x_d}\right)^\top = L_d x_d, \tag{28}$$

with $e_d =: \left((e_d^1)^\top \quad (e_d^2)^\top \quad (e_d^3)^\top\right)^\top$ where the $e_d^{\{1..3\}}$ are vectors of the same dimensions as their state counterparts $x_d^{\{1..3\}}$. One obtains, for the efforts on the (i, j)-indexed grid point,

$$\begin{pmatrix} e_{i,j}^1 \\ e_{i,j}^2 \\ e_{i,j}^3 \end{pmatrix} = \begin{pmatrix} \mu_0^{-1} & 0 & 0 \\ 0 & \mu_0^{-1} & 0 \\ 0 & 0 & \chi_s^{-1} \end{pmatrix} \begin{pmatrix} x_{i,j}^1 \\ x_{i,j}^2 \\ x_{i,j}^3 \end{pmatrix}. \tag{29}$$

Taking into account that

$$\begin{pmatrix} x_{i,j}^1 \\ x_{i,j}^2 \\ x_{i,j}^3 \end{pmatrix} \approx \begin{pmatrix} x^1(\xi_{i+0.5}^1, \xi_j^2) \\ x^2(\xi_i^1, \xi_{j+0.5}^2) \\ x^3(\xi_i^1, \xi_j^2) \end{pmatrix} \quad \text{and} \quad \begin{pmatrix} e_{i,j}^1 \\ e_{i,j}^2 \\ e_{i,j}^3 \end{pmatrix} \approx \begin{pmatrix} e^1(\xi_{i+0.5}^1, \xi_j^2) \\ e^2(\xi_i^1, \xi_{j+0.5}^2) \\ e^3(\xi_i^1, \xi_j^2) \end{pmatrix}$$

where $\xi_i^1 = ih_i$, $\xi_{i+0.5}^1 = (i+0.5)h_1$, $\xi_j^2 = jh_2$ and $\xi_{j+0.5}^2 = (j+0.5)h_2$, we obtain by central approximation of the spatial derivative the following numerical scheme

$$\begin{aligned} f_{i,j}^1 &= -\frac{1}{h_1}(e_{i+1,j}^3 - e_{i,j}^3), \\ f_{i,j}^2 &= -\frac{1}{h_2}(e_{i,j+1}^3 - e_{i,j}^3), \\ f_{i,j}^3 &= -\frac{1}{h_1}(e_{i,j}^1 - e_{i-1,j}^1) - \frac{1}{h_2}(e_{i,j}^2 - e_{i,j-1}^2). \end{aligned} \tag{30}$$

Define the vector of discrete flows as

$$\begin{aligned} f_d &= \left((f_d^1)^\top \quad (f_d^2)^\top \quad (f_d^3)^\top\right)^\top = \\ &\begin{pmatrix} f_{1,1}^1 & \cdots & f_{m-1,n}^1 & f_{1,1}^2 & \cdots & f_{m,n-1}^2 & f_{1,1}^3 & \cdots & f_{m,n}^3 \end{pmatrix}^\top. \end{aligned}$$

The vector f_d is the approximation of $\frac{\partial x_d}{\partial t}$ evaluated at the same spatial points as the state variables. The elements of f_d are hence given by

$$f_d^1 = \underbrace{-\frac{1}{h_1}\begin{pmatrix} -1 & 1 & & \\ & \ddots & \ddots & \\ & & -1 & 1 \end{pmatrix}}_{D_1} e_d^3 \tag{31}$$

where $D_1 \in \mathbb{R}^{n(m-1)\times mn}$,

$$f_d^2 = \underbrace{-\frac{1}{h_2}\begin{pmatrix} K_1 & & \\ & \ddots & \\ & & K_1 \end{pmatrix}}_{D_2} e_d^3 \tag{32}$$

where $D_2 \in \mathbb{R}^{m(n-1)\times mn}$ and

$$K_1 = \begin{pmatrix} -1 & 1 & & \\ & \ddots & \ddots & \\ & & -1 & 1 \end{pmatrix}, \tag{33}$$

$K_1 \in \mathbb{R}^{(n-1)\times n}$, $f_d^3 = f_{d1}^3 + f_{d2}^3$

$$f_{d1}^3 = -(D_1)^\top e_d^1 + \underbrace{\frac{1}{h_1}\begin{pmatrix} I_n & 0 \\ 0 & \vdots \\ \vdots & 0 \\ 0 & -I_n \end{pmatrix}}_{g_1} e_{d\partial}^1 \tag{34}$$

where $g_1 \in \mathbb{R}^{mn\times 2n}$, I_n the identity matrix of dimension n and

$$f_{d2}^3 = -(D_2)^\top e_d^2 + \underbrace{\frac{1}{h_2}\begin{pmatrix} K_2 & & \\ & \ddots & \\ & & K_2 \end{pmatrix}}_{g_2} e_{d\partial}^2 \tag{35}$$

where $g_2 \in \mathbb{R}^{mn\times 2m}$,

$$K_2 = \begin{pmatrix} 1 & 0 \\ 0 & \vdots \\ \vdots & 0 \\ 0 & -1 \end{pmatrix}$$

with $K_2 \in \mathbb{R}^{n\times 2}$. The discrete flow vector f_d becomes

$$f_d = \underbrace{\begin{pmatrix} 0 & 0 & D_1 \\ 0 & 0 & D_2 \\ -D_1^\top & -D_2^\top & 0 \end{pmatrix}}_{J_d} e_d + \underbrace{\begin{pmatrix} 0 & 0 \\ g_1 & g_2 \end{pmatrix}}_{g_d} \begin{pmatrix} e_{d\partial}^1 \\ e_{d\partial}^2 \end{pmatrix}. \tag{36}$$

Proposition 8. *The staggered-grid finite-difference spatial discretization of (21) according to the scheme (30) defines a finite-dimensional Dirac structure $\mathcal{D}_d$ which approximates the original Stokes Dirac structure. The approximated system*

$$\begin{cases} \dot{x}_d = J_d L_d x_d + g_d u_d \\ y_d = g_d^\top e_d \end{cases} \tag{37}$$

with $u_d = e_d^\partial$ and

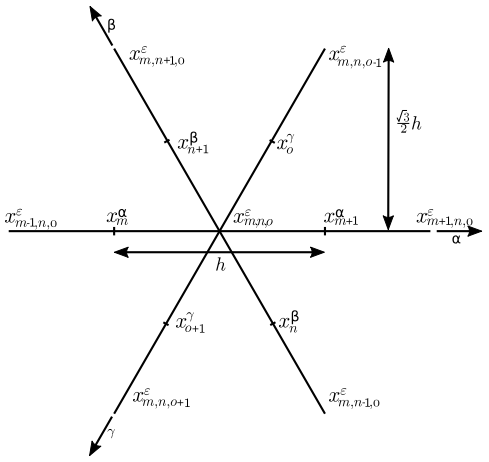

Fig. 4. Triangular staggered discretization for $x^{\alpha..\varepsilon}$.

$$y_d = f_d^{\partial} = \left(\tfrac{1}{h_1}e^3_{1,1}\ \tfrac{1}{h_1}e^3_{1,2}\ \cdots\ \tfrac{1}{h_1}e^3_{1,n}\ -\tfrac{1}{h_1}e^3_{m,1}\ -\tfrac{1}{h_1}e^3_{m,2}\ \cdots\ -\tfrac{1}{h_1}e^3_{m,n}\ \tfrac{1}{h_2}e^3_{1,1}\ -\tfrac{1}{h_2}e^3_{1,n}\ \tfrac{1}{h_2}e^3_{2,1}\ -\tfrac{1}{h_2}e^3_{2,n}\ \cdots\ \tfrac{1}{h_2}e^3_{m,1}\ -\tfrac{1}{h_2}e^3_{m,n}\right)^{\top}$$

is thus a PHS.

Proof. The proof of this proposition is analogous to the proof of Proposition 5 in the 1D case considering $e'_d = \begin{pmatrix} e_d \\ e_d^{\partial} \end{pmatrix} \in \mathbb{R}^{3mn+(m+n)}$ and $f'_d = \begin{pmatrix} f_d \\ f_d^{\partial} \end{pmatrix} \in \mathbb{R}^{3mn+(m+n)}$ according to (26) and (28). □

The energy balance of the discrete system, expressed in terms of boundary efforts and flows, is

$$\dot{H}_d(t) = (e_d^{\partial})^{\top} f_d^{\partial} = \sum_{i=1}^{m} \frac{1}{h_1}\left(e^2_{i,0}e^3_{i,1} - e^2_{i,n}e^3_{i,n}\right) + \sum_{j=1}^{n} \frac{1}{h_2}\left(e^1_{0,j}e^3_{1,j} - e^1_{m,j}e^3_{m,j}\right) \tag{38}$$

and $h_1 h_2 \dot{H}_d(t)$ converges to $\dot{\mathcal{H}}$ when m and n tend to infinity.

3.3. Regular triangular grids

A regular triangular staggered mesh leads to simple compact 7-point stencils for a better approximation of the solution. The use of three spatial axes for the characterisation of the wave propagation is more accurate considering the isotropy of the wave propagation. Note that the preservation of the isotropy is interesting only in a uniform domain, i.e., when μ_0 and χ_s are independent from the space variables. Indeed, in (18), the operator $\frac{1}{\chi_s} div\left(\frac{1}{\mu_0} grad(\cdot)\right)$ is isotropic only in the uniform case, where it becomes equivalent to $\frac{1}{\mu_0\chi_s}\Delta\cdot$ with Δ the Laplacian operator. Using a rectilinear or regular triangular mesh can represent a drawback when applied to complex geometries since the mesh doesn't necessarily match the physical geometry of the system. Here, using a regular triangular tiling on an system with a rectangular domain induces the definition of discrete points on each side of the physical boundary. For the sake of simplicity, a staircase approximation is considered in this work, i.e., that the nearest discrete point corresponds to the boundary. Recent works however [32,46] tackle this challenge by defining unstructured finite volume elements on the boundary to fit the physical geometry while using finite differences inside the domain.

Contrarily to the rectilinear case, and since we consider equilateral triangles in the proposed meshing, it is non trivial to impose different spatial steps for the different axes of the domain, as it is the case in the traditional Finite-Difference Time Domain (FDTD) method.

Remark 9. Even though in this work we don't consider complex geometries, a regular triangular mesh is generally more adapted to these cases since it allows to match more precisely the curvature of the boundaries of the considered spatial domain [46].

To perform a finite-difference discretization which preserves the port-Hamiltonian structure of (21), it is necessary to approximate the first order differential operators gradient and divergence. Three axes α, β, γ, are used to define the discrete points as shown in Fig. 4 where $h > 0 \in \mathbb{R}$ is the spatial step, identical for each axis. We denote by $\vec{u}_{\alpha}$, $\vec{u}_{\beta}$, $\vec{u}_{\gamma}$ the unitary vectors of these axes.

This results in the definition of a new set of state variables for the infinite-dimensional system, $(x_\alpha\ x_\beta\ x_\gamma\ x_\varepsilon)^\top$ where $x_{\{\alpha,\beta,\gamma\}}$ are linked to the state $(x_1\ x_2\ x_3)^\top$ by projection over the cartesian axes such that

$$x_\alpha := x_1, \qquad x_\beta := -\frac{1}{2}x_1 + \frac{\sqrt{3}}{2}x_2, \qquad x_\gamma := -\frac{1}{2}x_1 - \frac{\sqrt{3}}{2}x_2$$

and $x_\varepsilon := x_3$. The effort variables $(e_\alpha\ e_\beta\ e_\gamma\ e_\varepsilon)^\top$ are defined accordingly by performing the same projections of $(e_1\ e_2)^\top$. Note that the inverse transformation is

$$x_1 = x_\alpha, \qquad x_2 = \frac{1}{\sqrt{3}}(x_\beta - x_\gamma), \qquad x_3 = x_\epsilon.$$

The Hamiltonian is derived from (20) and is given by

$$H = \int_0^{L_1}\int_0^{L_2}\left[\frac{1}{3\mu_0}\left(x_\alpha^2 + x_\beta^2 + x_\gamma^2\right) + \frac{1}{2\chi_s}x_\varepsilon^2\right]d\xi_1 d\xi_2 \tag{39}$$

where the first term in the integral may be interpreted as the kinetic energy density, which is $\frac{1}{2\mu_0}(x_1^2 + x_2^2)$ in cartesian coordinates, and the second term the potential energy.

We propose to perform a centered finite-difference approximation on the gradient operator which leads to

$$\begin{aligned}
\frac{\partial x_3(\xi_{k+0.5}, \xi_l)}{\partial\alpha} &=: \frac{\partial x_\varepsilon(\alpha_{m+0.5}, \beta_n, \gamma_o)}{\partial\alpha} \approx \frac{x^\varepsilon_{m+1,n,o} - x^\varepsilon_{m,n,o}}{h},\\
\frac{\partial x_3(\xi_{k-0.25}, \xi_{l+\frac{\sqrt{(3)}}{4}})}{\partial\beta} &=: \frac{\partial x_\varepsilon(\alpha_m, \beta_{n+0.5}, \gamma_o)}{\partial\beta} \approx \frac{x^\varepsilon_{m,n+1,o} - x^\varepsilon_{m,n,o}}{h},\\
\frac{\partial x_3(\xi_{k+0.25}, \xi_{l+\frac{\sqrt{(3)}}{4}})}{\partial\gamma} &=: \frac{\partial x_\varepsilon(\alpha_m, \beta_n, \gamma_{o+0.5})}{\partial\gamma} \approx \frac{x^\varepsilon_{m,n,o+1} - x^\varepsilon_{m,n,o}}{h},
\end{aligned} \tag{40}$$

completed with the approximation of the divergence operator

$$\begin{aligned}
&\frac{\partial x_\alpha(\alpha_m, \beta_n, \gamma_o)}{\partial\alpha} + \frac{\partial x_\beta(\alpha_m, \beta_n, \gamma_o)}{\partial\beta} + \frac{\partial x_\gamma(\alpha_m, \beta_n, \gamma_o)}{\partial\gamma}\\
&\qquad \approx \frac{2}{3h}(x^\alpha_{m+1} - x^\alpha_m + x^\beta_{n+1} - x^\beta_n + x^\gamma_{o+1} - x^\gamma_0).
\end{aligned} \tag{41}$$

Remark 10. The left hand term in (41) is indeed equivalent to the traditional expression of divergence in Cartesian coordinates:

$$\begin{aligned}
&\frac{\partial x_\alpha}{\partial\alpha} + \frac{\partial x_\beta}{\partial\beta} + \frac{\partial x_\gamma}{\partial\gamma}\\
&= \frac{\partial x_\alpha}{\partial\xi_1}\frac{\partial\xi_1}{\partial\alpha} + \frac{\partial x_\alpha}{\partial\xi_2}\frac{\partial\xi_2}{\partial\alpha} + \frac{\partial x_\beta}{\partial\xi_1}\frac{\partial\xi_1}{\partial\beta} + \frac{\partial x_\beta}{\partial\xi_2}\frac{\partial\xi_2}{\partial\beta} + \frac{\partial x_\gamma}{\partial\xi_1}\frac{\partial\xi_1}{\partial\gamma} + \frac{\partial x_\gamma}{\partial\xi_2}\frac{\partial\xi_2}{\partial\gamma}\\
&= \frac{\partial x_1}{\partial\xi_1}\frac{\partial\xi_1}{\partial\alpha} - \frac{1}{2}\frac{\partial x_1}{\partial\xi_1}\frac{\partial\xi_1}{\partial\beta} + \frac{\sqrt{3}}{2}\frac{\partial x_2}{\partial\xi_2}\frac{\partial\xi_2}{\partial\beta} - \frac{1}{2}\frac{\partial x_1}{\partial\xi_1}\frac{\partial\xi_1}{\partial\gamma} - \frac{\sqrt{3}}{2}\frac{\partial x_2}{\partial\xi_2}\frac{\partial\xi_2}{\partial\gamma}\\
&= \frac{\partial x_1}{\partial\xi_1}\times 1 - \frac{1}{2}\frac{\partial x_1}{\partial\xi_1}\times 0 + \frac{\sqrt{3}}{2}\frac{\partial x_2}{\partial\xi_2}\frac{1}{\sqrt{3}} - \frac{1}{2}\frac{\partial x_1}{\partial\xi_1}\times 0 - \frac{\sqrt{3}}{2}\frac{\partial x_2}{\partial\xi_2}\frac{-1}{\sqrt{3}}\\
&= \frac{\partial x_1}{\partial\xi_1} + \frac{\partial x_2}{\partial\xi_2}.
\end{aligned}$$

Notice that the combination of the schemes (40) and (41) leads to the approximation of the Laplacian operator

$$\begin{aligned}
&\frac{\partial^2 x_\epsilon(\alpha_m, \beta_n, \gamma_o)}{\partial\alpha^2} + \frac{\partial^2 x_\epsilon(\alpha_m, \beta_n, \gamma_o)}{\partial\beta^2} + \frac{\partial^2 x_\epsilon(\alpha_m, \beta_n, \gamma_o)}{\partial\gamma^2}\\
&\qquad \approx \frac{2}{3h^2}\left(x^\epsilon_{m+1,n,o} + x^\epsilon_{m,n+1,o} + x^\epsilon_{m,n,o+1} + x^\epsilon_{m-1,n,o} + x^\epsilon_{m,n-1,o} + x^\epsilon_{m,n,o-1} - 6x^\epsilon_{m,n,o}\right),
\end{aligned} \tag{42}$$

which is symmetrical for each axis. Note that the scheme (42) is consistent with the finite-difference method applied on the order 2 wave equation [34,31].

The grid can then be described as the interconnection of elementary port-Hamiltonian systems defined by quadratic Hamiltonian functions representing the energy stored along the different axes

$$\Sigma_\alpha \begin{cases} H_m^\alpha = \frac{1}{2}\frac{2}{3h\mu_0}(x_m^\alpha)^2 \\ \dot{x}_m^\alpha = 0\frac{2}{3h\mu_0}x_m^\alpha + u_m^\alpha \\ y_m^\alpha = \frac{2}{3h\mu_0}x_m^\alpha \end{cases}, \quad \Sigma_\beta = \begin{cases} H_n^\beta = \frac{1}{2}\frac{2}{3h\mu_0}(x_n^\beta)^2 \\ \dot{x}_n^\beta = 0\frac{2}{3h\mu_0}x_n^\beta + u_n^\beta \\ y_n^\beta = \frac{2}{3h\mu_0}x_n^\beta \end{cases},$$
$$\Sigma_\gamma = \begin{cases} H_o^\gamma = \frac{1}{2}\frac{2}{3h\mu_0}(x_o^\gamma)^2 \\ \dot{x}_o^\gamma = 0\frac{2}{3h\mu_0}x_o^\gamma + u_o^\gamma \\ y_o^\gamma = \frac{2}{3h\mu_0}x_o^\gamma \end{cases}, \quad \Sigma_\varepsilon = \begin{cases} H_{m,no}^\varepsilon = \frac{1}{2}\frac{1}{h\chi_s}(x_{m,n,o}^\varepsilon)^2 \\ \dot{x}_{m,n,o}^\varepsilon = 0\frac{1}{h\chi_s}x_{m,n,o}^\varepsilon + u_{m,n,o}^\varepsilon \\ y_{m,n,o}^\varepsilon = \frac{1}{h\chi_s}x_{m,n,o}^\varepsilon \end{cases}, \tag{43}$$

interconnected in a power preserving way

$$\begin{pmatrix} u_m^\alpha \\ u_n^\beta \\ u_o^\gamma \\ u_{m,n,o}^\varepsilon \end{pmatrix} = \begin{pmatrix} 0_{3,3} & \begin{matrix}-1\\-1\\-1\end{matrix} \\ 1\ 1\ 1 & 0 \end{pmatrix} \begin{pmatrix} y_m^\alpha \\ y_n^\beta \\ y_o^\gamma \\ y_{m,n,o}^\varepsilon \end{pmatrix} + \begin{pmatrix} \frac{1}{h\chi_s}x_{m-1,n,o}^\varepsilon \\ \frac{1}{h\chi_s}x_{m,n-1,o}^\varepsilon \\ \frac{1}{h\chi_s}x_{m,n,o-1}^\varepsilon \\ -\frac{2}{3h\mu_0}(x_{m+1}^\alpha + x_{n+1}^\beta + x_{o+1}^\gamma) \end{pmatrix}. \tag{44}$$

On the triangular grid of Fig. 4, this leads to the system

$$\begin{pmatrix} \dot{x}_m^\alpha \\ \dot{x}_{m+1}^\alpha \\ \dot{x}_n^\beta \\ \dot{x}_{n+1}^\beta \\ \dot{x}_o^\gamma \\ \dot{x}_{o+1}^\gamma \\ \dot{x}_{m,n,o}^\varepsilon \end{pmatrix} = \begin{pmatrix} & & & & & & -1 \\ & & & & & & 1 \\ & & & 0_{6,6} & & & -1 \\ & & & & & & 1 \\ & & & & & & -1 \\ & & & & & & 1 \\ 1 & -1 & 1 & -1 & 1 & -1 & 0 \end{pmatrix} \begin{pmatrix} \frac{2}{3h\mu_0}I_{6,6} & 0 \\ 0 & \frac{1}{h\chi_s} \end{pmatrix} \begin{pmatrix} x_m^\alpha \\ x_{m+1}^\alpha \\ x_n^\beta \\ x_{n+1}^\beta \\ x_o^\gamma \\ x_{o+1}^\gamma \\ x_{m,n,o}^\varepsilon \end{pmatrix} + \begin{pmatrix} I_{6,6} \\ 0_{1,6} \end{pmatrix} \begin{pmatrix} \frac{l_2}{h}x_{m-1,n,o}^\varepsilon \\ -\frac{l_2}{h}x_{m+1,n,o}^\varepsilon \\ \frac{l_2}{h}x_{m,n-1,o}^\varepsilon \\ -\frac{l_2}{h}x_{m,n+1,o}^\varepsilon \\ \frac{l_2}{h}x_{m,n,o-1}^\varepsilon \\ -\frac{l_2}{h}x_{m,n,o+1}^\varepsilon \end{pmatrix}$$
$$\begin{pmatrix} x_m^\alpha \\ x_{m+1}^\alpha \\ x_n^\beta \\ x_{n+1}^\beta \\ x_o^\gamma \\ x_{o+1}^\gamma \end{pmatrix} = \begin{pmatrix} I_{6,6} & 0_{6,1} \end{pmatrix} \begin{pmatrix} x_m^\alpha \\ x_{m+1}^\alpha \\ x_n^\beta \\ x_{n+1}^\beta \\ x_o^\gamma \\ x_{o+1}^\gamma \\ x_{m,n,o}^\varepsilon \end{pmatrix}. \tag{45}$$

Consider now the discretization of system (21). The same rectangular domain and boundary conditions as for the rectilinear meshing are considered. This leads to impose either e_α, e_β or e_γ at the boundary of the spatial domain. The choice of the spatial step h can induce several configurations of the triangular mesh and thus leads to a number of triangles along the ξ_2 axis which can be odd or even. An example of regular triangular mesh for this system is shown in Fig. 5 for an even number of triangles per column. However, the following development holds for any h, and thus also for an odd number of triangles per column.

Define by $n_{tl} \in \mathbb{N}$ the number of triangles of the same orientation per line and $n_{tc} \in \mathbb{N}$ the total number of triangles per column. Notice that the numbering $x_{m,n,o}^\varepsilon$ is redundant since it implies that several indexes can correspond to the same point, for instance $x_{m,n-1,o}^\varepsilon = x_{m+1,n,o+1}^\varepsilon$. Hence one cannot express the interconnection of the scheme as defined on Fig. 4 to derive a complete grid. It is thus necessary to define a new numbering of the discrete points. The simplest way is to consider the numbering described in Fig. 6. The positions of the points of each different nature are described by an index which is incremented from left to right, and from top to bottom.

From n_{tl}, n_{tc}, define n_α, n_β, n_γ and n_ε the number of points where x_α, x_β, x_γ and x_ε are approximated, respectively,

$$n_\alpha = n_{tl}(n_{tc}+1)$$
$$n_\beta = \begin{cases} (n_{tl}+0.5)n_{tc} \text{ if } n_{tc} \text{ even} \\ 0.5((n_{tl}+1)(n_{tc}+1) + (n_{tl}(n_{tc}-1)) \text{ if } n_{tc} \text{ odd} \end{cases}$$
$$n_\gamma = \begin{cases} (n_{tl}+0.5)n_{tc} \text{ if } n_{tc} \text{ even} \\ 0.5(n_{tl}(n_{tc}+1) + ((n_{tl}+1)(n_{tc}-1)) \text{ if } n_{tc} \text{ odd} \end{cases}$$
$$n_\varepsilon = (n_{tl}+1)(n_{tc}+1).$$

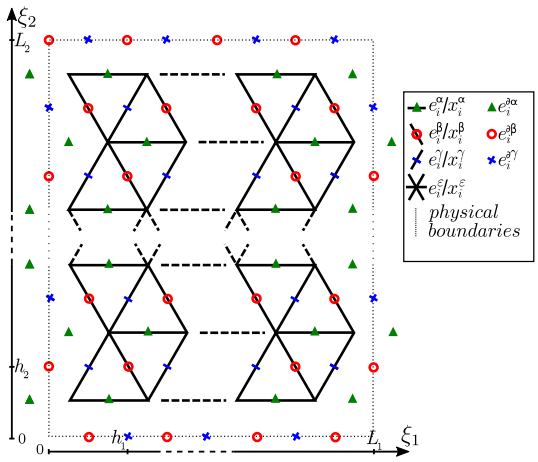

Fig. 5. Example of regular triangular staggered meshing for state/effort discretization.

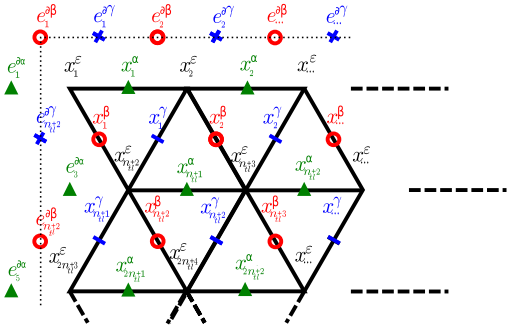

Fig. 6. Numbered regular triangular staggered meshing for state/effort discretization.

Define the total number of points $n_d = \Sigma n_{\{\alpha,\beta,\gamma,\varepsilon\}}$. The finite-dimensional state vector is

$$x_d = ((x_d^\alpha)^\top \ (x_d^\beta)^\top \ (x_d^\gamma)^\top \ (x_d^\varepsilon)^\top)^\top \in \mathbb{R}^{n_d}$$

with

$$x_d^\alpha = (x_1^\alpha \ \dots \ x_{n_\alpha}^\alpha)^\top, \qquad x_d^\beta = (x_1^\beta \ \dots \ x_{n_\beta}^\beta)^\top,$$
$$x_d^\gamma = (x_1^\gamma \ \dots \ x_{n_\gamma}^\gamma)^\top, \qquad x_d^\varepsilon = (x_1^\varepsilon \ \dots \ x_{n_\varepsilon}^\varepsilon)^\top.$$

Similarly, derive from n_{tl} and n_{tc} the numbers $n^\partial_{\{\alpha..\varepsilon\}}$ of boundary points for each imposed effort $e^{\partial\{\alpha..\varepsilon\}}$

$$\begin{aligned} n_\alpha^\partial &= 2(n_{tc}+1) \\ n_\beta^\partial &= 2(n_{tl}+1) + \begin{cases} n_{tc} \text{ if } n_{tc} \text{ even} \\ n_{tc}-1 \text{ if } n_{tc} \text{ odd} \end{cases} \\ n_\gamma^\partial &= 2(n_{tl}+1) + \begin{cases} n_{tc} \text{ if } n_{tc} \text{ even} \\ n_{tc}+1 \text{ if } n_{tc} \text{ odd} \end{cases} \\ n_\varepsilon^\partial &= 0, \end{aligned} \tag{46}$$

and the total number of boundary points $n_d^\partial = \Sigma n^\partial_{\{\alpha..\varepsilon\}}$. The boundary effort variables are

$$e_d^\partial = ((e_{d\partial}^\alpha)^\top \ (e_{d\partial}^\beta)^\top \ (e_{d\partial}^\gamma)^\top \ (e_{d\partial}^\varepsilon)^\top)^\top \in \mathbb{R}^{n_d^\partial} \tag{47}$$

with

$$e_{d\partial}^\alpha = (e_1^{\partial\alpha} \ \dots \ e_{n_\alpha^\partial}^{\partial\alpha})^\top, \qquad e_{d\partial}^\beta = (e_1^{\partial\beta} \ \dots \ e_{n_\beta^\partial}^{\partial\beta})^\top,$$
$$e_{d\partial}^\gamma = (e_1^{\partial\gamma} \ \dots \ e_{n_\gamma^\partial}^{\partial\gamma})^\top, \qquad e_{d\partial}^\varepsilon = (e_1^{\partial\varepsilon} \ \dots \ e_{n_\varepsilon^\partial}^{\partial\varepsilon})^\top.$$

The discrete Hamiltonian H_d is defined as

$$H_d := \frac{1}{2} x_d L_d x_d \tag{48}$$

where $L_d \in \mathbb{R}^{n_d \times n_d}$ is a diagonal matrix which corresponds to the evaluation on the grid points of $\begin{pmatrix} \frac{2}{3} & 0 \\ 0 & 1 \end{pmatrix} \mathcal{L}$. Note that $h^2 H_d \approx H$ in the sense that $h^2 H_d$ converges to H when the number of points tends to infinity. This permits to define the discrete effort as

$$e_d := \frac{\partial H_d}{\partial x_d} = L_d x_d. \tag{49}$$

In order to define the flow variables we introduce some additional notation. Define the matrices

$$K_1 = \begin{pmatrix} -1 & 1 & & \\ & \ddots & \ddots & \\ & & -1 & 1 \end{pmatrix}, \qquad K_2 = I_{n_{tl}+1}, \qquad K_3 = \begin{pmatrix} & 0 \\ I_{n_{tl}} & \vdots \\ & 0 \end{pmatrix}, \qquad K_4 = \begin{pmatrix} 0 & \\ \vdots & I_{n_{tl}} \\ 0 & \end{pmatrix},$$

where $\{K_1, K_2, K_4\} \in \mathbb{R}^{n_{tl} \times (n_{tl}+1)}$. The differential operator $\frac{\partial}{\partial \alpha}$ is approximated by the matrix

$$D_1 = \frac{1}{h} \begin{pmatrix} K_1 & & \\ & \ddots & \\ & & K_1 \end{pmatrix}$$

$D_1 \in \mathbb{R}^{n_\alpha \times n_\varepsilon}$. The operator $\frac{\partial}{\partial \beta}$ is approximated by the matrix $D_2 = D_2^+ - D_2^-$ with

$$D_2^+ = \frac{1}{h} \begin{pmatrix} K_2 & & & & \\ & K_3 & & & \\ & & K_2 & & \mathbf{0}_{n_b, n_{tl}+1} \\ & & & \ddots & \end{pmatrix}, \qquad D_2^- = \frac{1}{h} \begin{pmatrix} & & K_2 & & \\ & & & K_4 & \\ \mathbf{0}_{n_b, n_{tl}+1} & & & K_2 & \\ & & & & \ddots \end{pmatrix}$$

$\{D_2, D_2^+, D_2^-\} \in \mathbb{R}^{n_\beta \times n_\varepsilon}$. The differential operator $\frac{\partial}{\partial \gamma}$ is approximated by the matrix $D_3 = D_3^+ - D_3^-$ with

$$D_3^+ = \frac{1}{h} \begin{pmatrix} & K_3 & & & \\ & & K_2 & & \\ \mathbf{0}_{n_c, n_{tl}+1} & & & K_3 & \\ & & & & \ddots \end{pmatrix}, \qquad D_3^- = \frac{1}{h} \begin{pmatrix} K_4 & & & & \\ & K_2 & & & \\ & & K_4 & & \mathbf{0}_{n_c, n_{tl}+1} \\ & & & \ddots & \end{pmatrix} \tag{50}$$

$\{D_3, D_3^+, D_3^-\} \in \mathbb{R}^{n_\gamma \times n_\varepsilon}$. Furthermore, we define the matrices

$$K_1^\partial = \begin{pmatrix} 1 & 0 \\ \mathbf{0}_{(n_{tl}-1),2} & \\ 0 & -1 \end{pmatrix}, \qquad K_2^\partial = \begin{pmatrix} \mathbf{0}_{n_{tl},2} & \\ 0 & 1 \\ -1 & 0 \\ \mathbf{0}_{n_{tl},2} & \end{pmatrix}, \qquad K_3^\partial = \begin{pmatrix} -1 & 0 \\ \mathbf{0}_{2n_{tl},2} & \\ 0 & 1 \end{pmatrix},$$

$$K_4^\partial = \begin{pmatrix} K_2^\partial & & \\ & \ddots & \\ & & K_2^\partial \end{pmatrix}, \qquad K_5^\partial = \begin{pmatrix} K_3^\partial & & \\ & \ddots & \\ & & K_3^\partial \end{pmatrix},$$

where[3] $K_4^\partial \in \mathbb{R}^{2(n_{tl}+1)\lfloor n_{tc}/2 \rfloor \times 2\lfloor n_t c/2 \rfloor}$ and $K_5^\partial \in \mathbb{R}^{2(n_{tl}+1)\lceil n_{tc}/2 \rceil \times 2\lceil n_t c/2 \rceil}$. Define the matrix

$$g_d = \frac{2}{3} \frac{1}{h} \begin{pmatrix} \mathbf{0}_{n_\alpha + n_\beta + n_\gamma, n_d^\partial} \\ g_\alpha \;\; g_\beta \;\; g_\gamma \end{pmatrix}$$

$g_d \in \mathbb{R}^{n_d \times n_d^\partial}$, where

[3] $\lfloor \cdot \rfloor$ and $\lceil \cdot \rceil$ are the floor function and the ceiling function, respectively.

$$g_\alpha = \begin{pmatrix} K_1 & & \\ & \ddots & \\ & & K_1 \end{pmatrix}$$

$$g_\beta = \begin{pmatrix} 0_{n_{tl}+1} & & & & \\ & K_4^\partial & 0 & & \\ & & \ddots & & \\ & & & 0 & \end{pmatrix} + \begin{pmatrix} -I_{n_{tl}+1} & & & & \\ & 0 & & & \\ & & \ddots & & \\ & & & 0 & \\ & & & & I_{n_{tl}+1} \end{pmatrix}$$

$$g_\gamma = \begin{pmatrix} 0_{n_{tl}+1} & & & & \\ & K_5^\partial & 0 & & \\ & & \ddots & & \\ & & & 0 & \end{pmatrix} + \begin{pmatrix} -I_{n_{tl}+1} & & & \\ & \ddots & & \\ & & & I_{n_{tl}+1} \end{pmatrix}$$

$g_\alpha \in \mathbb{R}^{n_\varepsilon, n_\alpha^\partial}$, $g_\beta \in \mathbb{R}^{n_\varepsilon, n_\beta^\partial}$ and $g_\gamma \in \mathbb{R}^{n_\varepsilon, n_\gamma^\partial}$. We also define

$$J_d = \begin{pmatrix} & \ddots & & -D_1 \\ & & & -D_2 \\ & & & -D_3 \\ D_1^\top & D_2^\top & D_3^\top & \ddots \end{pmatrix}.$$

The discrete vector $f_d = \frac{dx_d}{dt}$ is then given by

$$f_d = J_d e_d + g_d e_d^\partial.$$

Proposition 11. *The staggered-grid finite-difference spatial discretization of (21) according to the scheme (40), (41) defines a finite-dimensional Dirac structure $\mathcal{D}_d$ which approximates the original Stokes Dirac structure. The approximated system*

$$\begin{cases} \dot{x}_d = J_d L_d x_d + g_d u_d \\ y_d = g_d^\top e_d \end{cases} \tag{51}$$

with $u_d = e_d^\partial$ is thus a PHS. $y_d = f_d^\partial$ with

$$f_d^\partial = g_{d1}^\top e_d^\partial = \frac{1}{h}((f_{d\partial}^\alpha)^\top (f_{d\partial}^\beta)^\top (f_{d\partial}^\gamma)^\top (f_{d\partial}^\varepsilon)^\top)^\top$$

where

$$\begin{aligned} f_{d\partial^\alpha}^\top =& \frac{2}{3}(e_1^\varepsilon - e_{n_{tl}+1}^\varepsilon\, e_{(n_{tl}+1)+1}^\varepsilon - e_{2(n_{tl}+1)}^\varepsilon\, e_{2(n_{tl}+1)+1}^\varepsilon \\ & \cdots e_{n_{tc}(n_{tl}+1)+1}^\varepsilon - e_{(n_{tc}+1)(n_{tl}+1)}^\varepsilon)^\top \\ f_{d\partial^\beta}^\top =& \frac{2}{3}(-e_1^\varepsilon \cdots - e_{n_{tl}+1}^\varepsilon - e_{2(n_{tl}+1)+1}^\varepsilon\, e_{2(n_{tl}+1)}^\varepsilon - e_{4(n_{tl}+1)+1}^\varepsilon \\ & e_{4(n_{tl}+1)}^\varepsilon \cdots e_{(n_{tc})(n_{tl}+1)+1}^\varepsilon \cdots e_{(n_{tc}+1)(n_{tl}+1)}^\varepsilon)^\top \\ f_{d\partial^\gamma}^\top =& \frac{2}{3}(e_1^\varepsilon \cdots e_{n_{tl}+1}^\varepsilon - e_1^\varepsilon\, e_{2(n_{tl}+1)}^\varepsilon - e_{2(n_{tl}+1)+1}^\varepsilon \\ & - e_{4(n_{tl}+1)}^\varepsilon \cdots - e_{(n_{tc})(n_{tl}+1)+1}^\varepsilon \cdots - e_{(n_{tc}+1)(n_{tl}+1)}^\varepsilon)^\top \end{aligned}$$

$f_{d\partial^\alpha} \in \mathbb{R}^{n_\alpha^\partial}$, $f_{d\partial^\beta} \in \mathbb{R}^{n_\beta^\partial}$ and $f_{d\partial^\gamma} \in \mathbb{R}^{n_\gamma^\partial}$. $f_{d\partial^\varepsilon}$ is equal to the empty set in the particular case due to the choice of the boundary conditions.

Proof. The proof of this proposition is analogous to the proof of the Proposition 5 in the 1D case considering $e_d' = \begin{pmatrix} e_d \\ e_d^\partial \end{pmatrix} \in \mathbb{R}^{n_d + n_d^\partial}$ and $f_d' = \begin{pmatrix} f_d \\ f_d^\partial \end{pmatrix} \in \mathbb{R}^{n_d + n_d^\partial}$ according to (47) and (49). □

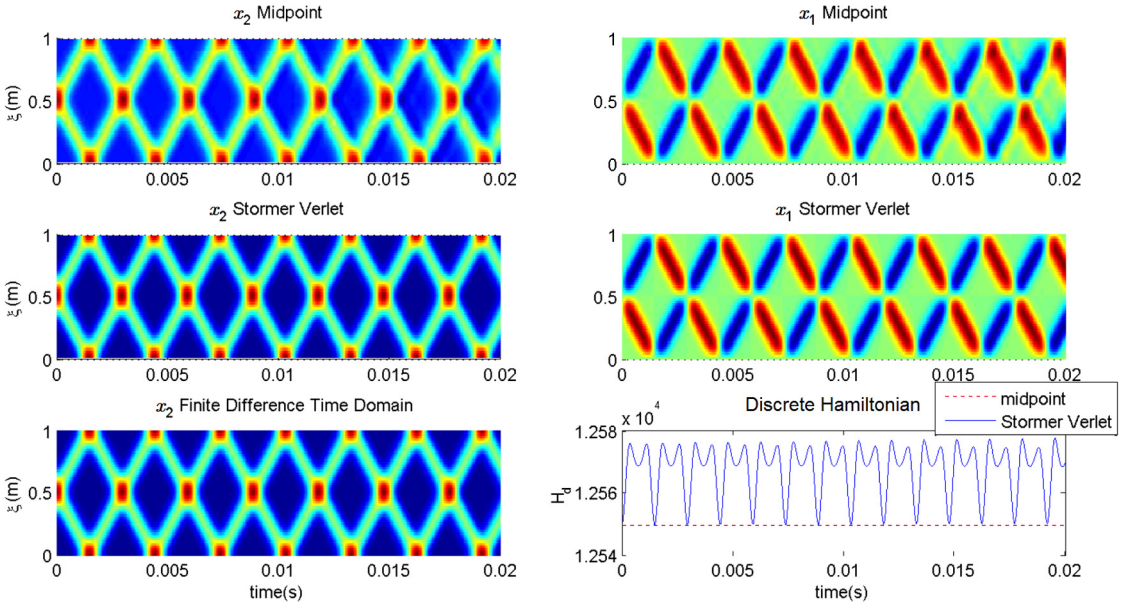

Fig. 7. 1D propagation of a Gaussian initial condition, comparison with traditional finite-difference time domain method, time step $\tau = 44.4\ \mu s$, $h = 2.0\ cm$.

4. Numerical experiment

In this section, the proposed discretization methods are implemented using MATLAB®. Advantages and limitations of the different numerical schemes are highlighted in a open-loop case and in a closed-loop case considering a fully absorbing boundary control. Since acoustic wave propagation in the air is considered we use the following physical parameters

$$\frac{1}{\mu_0} = 0.8163\ m^3.kg^{-1}, \qquad \frac{1}{\chi_s} = 1.4161.10^5\ Pa, \qquad c_0 = 340\ m.s^{-1} \tag{52}$$

We recall that μ_0 is the mass density and χ_s is the adiabatic compressibility factor. The proposed discretization method is completed with midpoint rule for the time integration, which coincide with the discrete gradient in the linear case, and thus respect the power balance of the system [36,47]. A short recall of the considered time integration methods is given in appendix.

4.1. 1D case – open-loop system

The propagation of a Gaussian initial condition in the center of the 1D spatial domain with fully reflective boundary conditions ($e^1_{d\partial} = 0$) is studied in Fig. 7.

We consider spatial step $h = 2\ cm$ and a spatial domain of length $L = 1\ m$. We simulate the system over a time $T = 20\ ms$ with a time step $\tau = 44.4\ \mu s$. The spatial step is chosen such that we can see significative differences between the different methods. The two first subfigures represent the state variables approximated with the staggered-grid method and implemented using the explicit PHS (15) with implicit midpoint time integration. In the second line of subfigures a Störmer–Verlet time integration [35] scheme is used. This is a two-step symplectic second order scheme for systems with separable Hamiltonian.

In the bottom left corner subfigure a full discretization using a finite-difference time domain method is performed on the order 2 wave equation (1). Bottom right corner subfigure shows the total energy of the system for midpoint and Störmer–Verlet integration. Fig. 7 shows some of the advantages of the proposed staggered-grid semi-discretization scheme over the FDTD method. In particular, the whole state of the system is made explicit and it is possible to compute the total energy directly from the states variables. Some numerical dispersion can be observed, especially for the midpoint integration method since the time step is not sufficiently small. The dispersion can be observed through the degradation of the patterns along time. Fig. 8, a zoom of Fig. 7, permits to see this degradation between the first and last observable patterns described by the simulated wave for the approximation of x_2 in the cases of a Störmer–Verlet and of a midpoint time integration. The results suggest that if the numerical dispersion is too important using the midpoint scheme the Störmer–Verlet integration scheme can be used instead. However, as it can be observed in the last subfigure, the price of less dispersion is that the total energy of the system, which should remain constant in this conservative system, oscillates with a relative error of about 0.3 per cent. The midpoint method is then used in the following.

In the following subsection the discretization is illustrated when a boundary controller is considered.

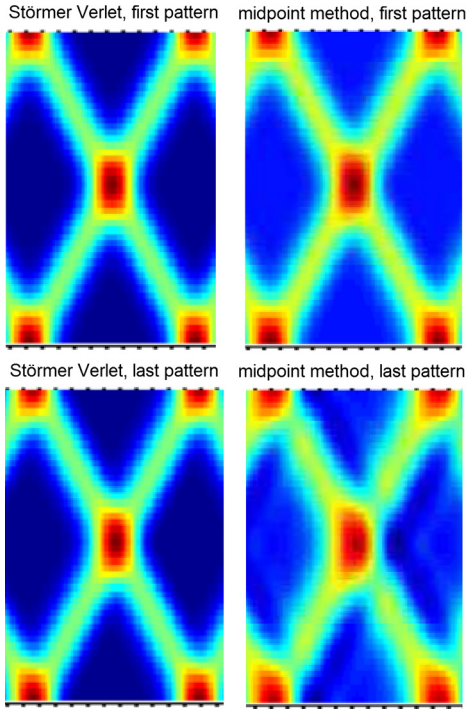

Fig. 8. Zoom of Fig. 7, degradation of the pattern due to dispersion for Midpoint and Störmer Verlet schemes.

4.2. 1D case – boundary control

The propagation of the same Gaussian initial condition is now considered in closed loop, with a boundary controller implemented at the $\xi = L = 1$ boundary. The simulation is performed for a time of $T = 10\ ms$ and a time step $\tau = 5\ \mu s$ for a spatial step $h = 2\ cm$. An impedance matching controller corresponding to fully absorbing boundary control [48] is considered. The control law is implemented by imposing the boundary condition

$$e_d^\partial(2) = -\frac{h}{\mu_0 c_0} f_d^\partial(2),$$

that can also be interpreted as the interconnection of the discretized wave equation (15) with the static controller

$$y_c = \frac{1}{\mu_0 c_0} h u_c, \qquad \begin{pmatrix} e_d^\partial(1) \\ e_d^\partial(2) \\ u_c \end{pmatrix} = \begin{pmatrix} 0 & 0 & 0 \\ 0 & 0 & -1 \\ 0 & 1 & 0 \end{pmatrix} \begin{pmatrix} f_d^\partial(1) \\ f_d^\partial(2) \\ y_c \end{pmatrix} \tag{53}$$

where $e_d^\partial(i)$ and $f_d^\partial(i)$ are the i^{th} components of the vectors e_d^∂ and f_d^∂, respectively. Fig. 9 illustrates the closed-loop system behavior and shows the evolution of the approximated total energy.

It can be seen that approximately half of the energy is dissipated each time the propagating initial condition hits the $\xi = 1$ boundary, which corresponds to the behavior of a fully absorbing boundary. Since traditional methods such as FDTD do not allow to impose directly the effort variables at the boundary, they cannot be used in a straightforward manner to study the performance of this type of control. This is one the main advantages in preserving the PHS structure, the fact that the input-output ports of the system correspond to physical variables that can be interconnected with for instance a boundary controller.

4.3. 2D case

In the following, numerical results for the $2D$ PH model using the rectilinear discretization developed in Subsection 3.2 and the regular triangular discretization developed in Subsection 3.3 are presented. In the considered physical context, the effort variables e^3 and e^ε represent the components of the acoustic pressure p. The system is simulated for a time $T = 0.2\ s$ with a time step $\tau = 0.6\ ms$. The same number of discrete points is used in the rectilinear and triangular cases $n_{tl} + 1 = m = 50$, $n_{tc} + 1 = n = 5$ with unitary spatial steps $h = h_1 = h_2 = 1\ m$. The considered input is a sinusoidal plane wave injected into the domain through the $\xi_1 = 0$ boundary and chosen equal to $sin(2\pi \frac{c}{\lambda})$ with wavelength $\lambda = \frac{L_1}{5}$, which implies that the length of the domain L_1 is a multiple of λ. This choice, combined with the replacement of the anechoic

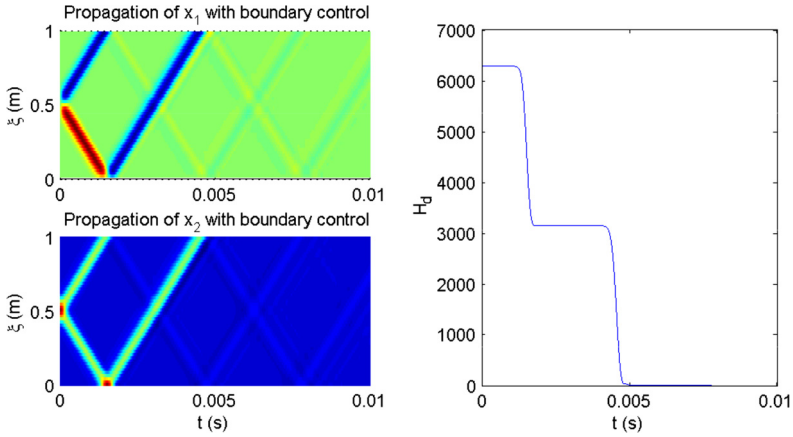

Fig. 9. 1D propagation of a Gaussian initial condition with boundary control and evolution of the discrete Hamiltonian, $\tau = 5\ \mu s$, $h = 2\ cm$.

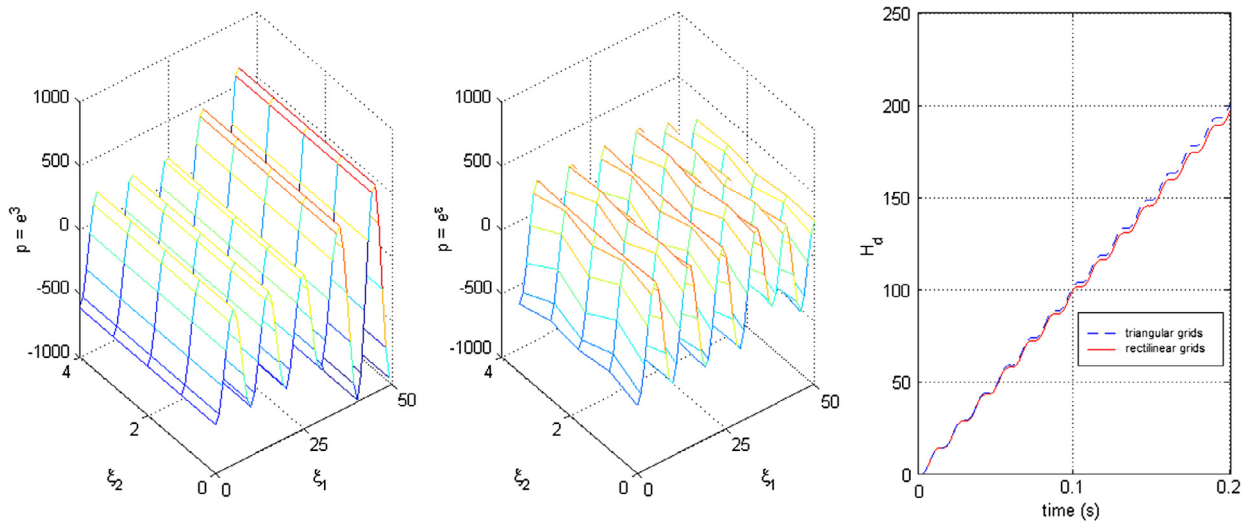

(a) Rectilinear grids (b) Triangular grids (c) Hamiltonian

Fig. 10. Propagation of a plane wave in open loop. (a) and (b): Snapshots at time $t = 0.2$s of e^3 and e^ε, respectively. (c): Evolution of the discrete Hamiltonian.

termination considered in Fig. 1 by a fully reflective condition, is the worst case scenario for the triangular case. Indeed, the reflection of the wave on the $\xi_1 = L_1$ boundary induces a perfectly constructive interference which cannot be simulated using the regular triangular mesh because of the staircase approximation on this boundary.

Figs. 10 and 11 present the simulations in open and closed loop, respectively. In these figures the 3D plots show the profiles of p at $t = 0.2s$. Fig. 10 shows that the approximation of the total energy in open loop for both discretization schemes are similar. The differences between the two curves is due to the staircase approximation at the $\xi_1 = L_1$ boundary for the triangular case. Indeed, this approximation does not preserve the shape of the reflected wave in this worst case scenario. It is unsurprising since the triangular mesh is more adapted to complex geometries. For the 2D case, the control law is similar to the fully absorbing condition presented in the 1D case. It is applied on a portion of the $\xi_2 = 0$ boundary along the ξ_1 axis. More precisely on the segment $\xi_1 \in \left[\frac{L_1}{3}, \frac{2L_1}{3}\right]$ as shown Fig. 12. The control law is implemented by using the boundary condition $e_2(\xi_1, 0, t) = \mu_0 c_0 e_3(\xi_1, 0, t)$.

Fig. 11 shows that in closed loop, the simulation using triangular mesh leads to a better dissipation of the energy of the system. Indeed, along the $\xi_1 = 0$ boundary where there is no staircase approximation needed and since the triangular mesh provides a better numerical propagation due to its compactness, we can expect the energy variation due to the absorbing control along $\xi_1 = 0$ to be more accurate. This is particularly important when considering passivity-based controllers [4,1,49] which are commonly based on energy dissipation.

In order to evaluate numerically the frequency response of the approximation in terms of the number of discretization points the Bode magnitude plots for the different approximations are drawn. Fig. 13 and Fig. 14 consider the approximation on rectilinear and triangular meshes, respectively.

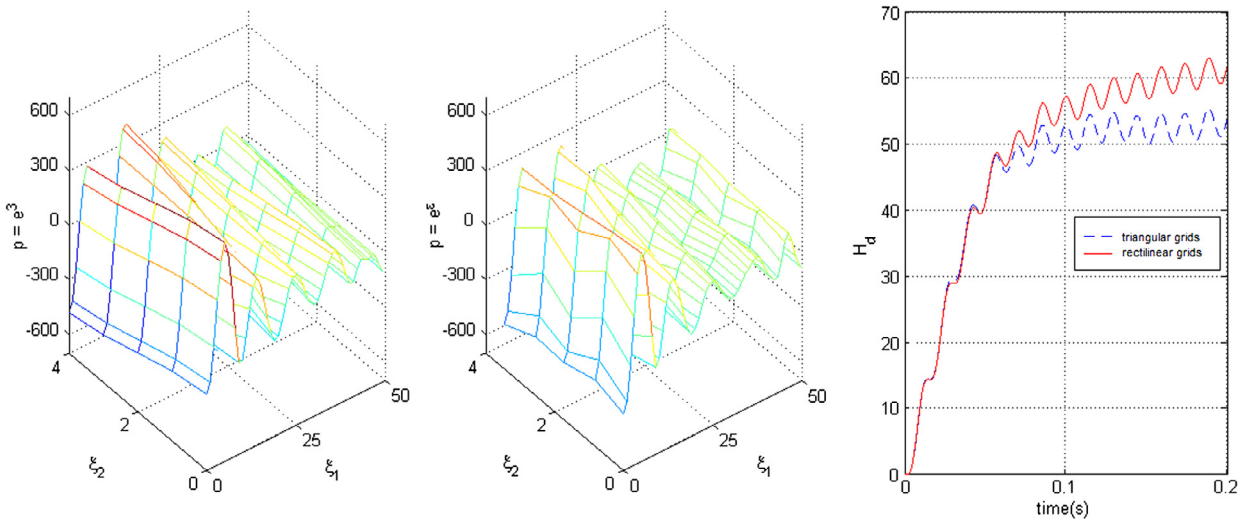

(a) Rectilinear grids (b) Triangular grids (c) Hamiltonian

Fig. 11. Propagation of a plane wave in closed loop. (a) and (b): Snapshots at time $t = 0.2$s of e^3 and e^ε, respectively. (c): Evolution of the discrete Hamiltonian.

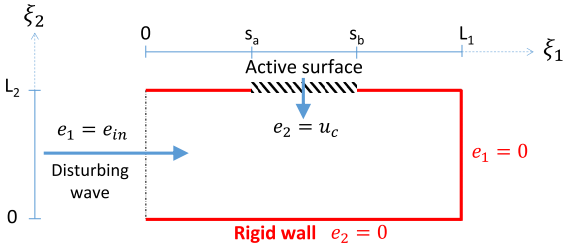

Fig. 12. Schematic representation of the spatial domain with boundary actuation.

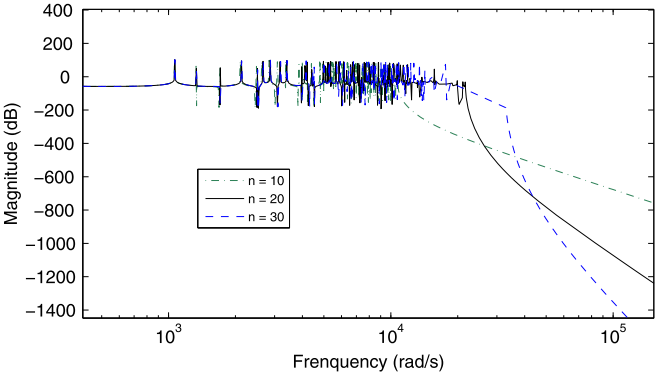

Fig. 13. Magnitude Bode of $\frac{e^3(L_1,\frac{L_2}{2})}{e^1(0,\frac{L_2}{2})}$ diagram for rectilinear discretization.

The considered inputs are the discrete approximation of $e^1(0,\frac{L_2}{2})$ in the rectilinear case, respectively $e^\alpha(0,\frac{L_2}{2})$ in the triangular case. The considered outputs are the discrete approximation of $e^3(L_1,\frac{L_2}{2})$ in the rectilinear case, respectively $e^\varepsilon(0,\frac{L_2}{2})$ in the triangular case. These choices correspond to the centers of opposite boundaries.

The cut-off frequency becomes higher when the number of points in the mesh is increased. The resulting roll-off also increases with the number of points. The shapes of the Bode plots are similar for the rectilinear and triangular cases, with some anti-resonances after the cut-off for the triangular case. These diagrams permit to evaluate numerically if the number of points used for the discretization is enough to study the system behavior up to a certain frequency.

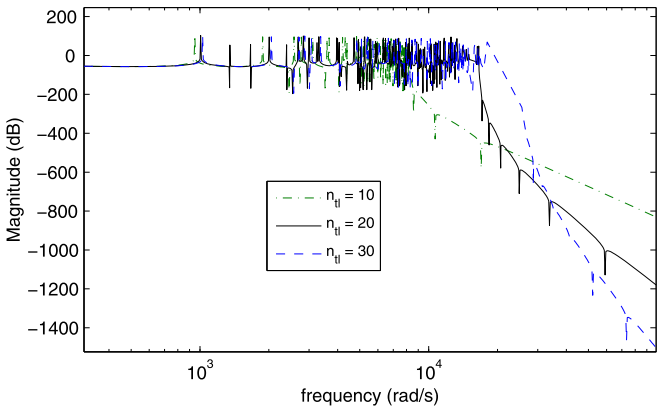

Fig. 14. Magnitude Bode diagram of $\frac{e^{\varepsilon}(0,\frac{L_2}{2})}{e^{u}(0,\frac{L_2}{2})}$ for regular triangular discretization.

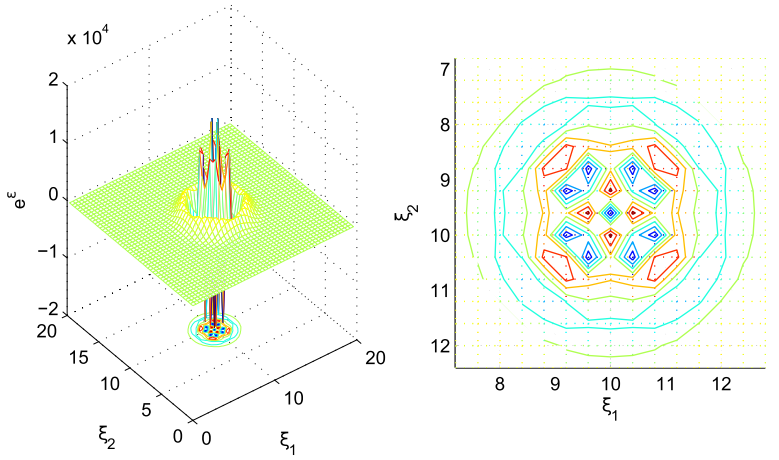

Fig. 15. Isolines (solid lines) of a propagation of an initial condition on a discrete point with rectilinear grids, $\tau = 1\ ms$, $t = 10\tau$, $h_1 = h_2 = 0.4\ m$.

4.4. Isotropy consideration

Figs. 15 and 16 show the contour plot, i.e., the isolines, of the propagation of a punctual initial condition at the center of a 2D domain with $L_1 = L_2 = 20\ m$. These figures show the profiles of p at $t = 10\tau$ with $\tau = 1\ ms$. The spatial steps are chosen such that the discretization leads to matrices J_d of almost the same size for both rectilinear and triangular cases, which permits to compare the two meshes at equivalent computation time. This is achieved by choosing $h_1 = h_2 = 0.4\ m$ for the rectilinear case and $h = 0.5\ m$ for the triangular case which lead to $J_d \in \mathbb{R}^{7400\times7400}$ and $J_d \in \mathbb{R}^{7371\times7371}$, respectively.

The figures show that the triangular mesh provides a better approximation of the isotropic propagation of the wave equation. Since the initial condition is applied on a point of the domain, the differences in the 3D plots are explained by the bad performance of finite differences for high frequencies. This suggests that regardless of the geometry of the studied system, if the interest is to study the behavior with respect to initial conditions the use of a regular triangular mesh is more convenient. Recall that to obtain these performances for a computing time equivalent to the rectilinear mesh, the price to pay for the use of the triangular mesh is a greater complexity of implementation.

5. Conclusion

A full discretization has been proposed for open systems governed by the wave equation in the 1D and 2D cases. The proposed spatial discretization scheme is based on staggered-grid finite differences such that it preserves the port-Hamiltonian structure of the system. Among the advantages of preserving the PHS structure, is that it allows to impose effort variables as boundary conditions on the finite-dimensional approximations and perform interconnections with subsystems such as boundary controllers. The main interest of the proposed method over other structure preserving discretization methods, such as mixed finite elements or structure preserving finite volumes, is its simplicity. In 2D, rectilinear and regular triangular meshes are treated. The time integration is based on the midpoint rule and has been specialized for a large class of linear PHS. It thus applies to the boundary interconnection of the proposed semi-discretized wave equation with linear

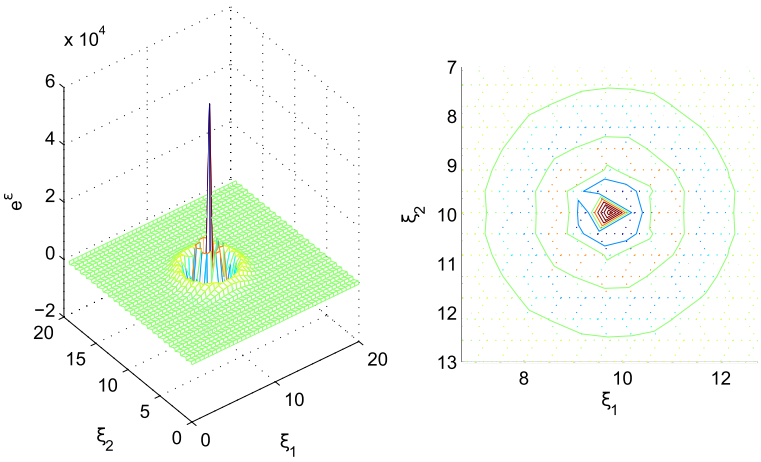

Fig. 16. Isolines (solid lines) of a propagation of an initial condition on a discrete point with triangular grids, $\tau = 1\ ms$, $t = 10\tau$, $h = 0.5\ m$.

PHS such as controllers. The numerical results show the convenience of the proposed methods for the 1D and 2D cases considering simulations in open and close loop, and illustrate the advantage of a regular triangular mesh over a rectilinear one regarding the isotropy of the wave propagation. A drawback of staggered-grid finite-difference discretization is that it is results in high complexity when considering unstructured meshes. In that sense, it loses its main advantage over other structure preserving discretization methods in this particular case. Future works will consider the extension of this method to 3D, *e.g.* for Maxwell's equations or room acoustic study, and the study of the interconnection of the proposed structured meshes with unstructured meshes, *e.g.* finite volumes such that the PHS structure of the system would be preserved. This will allow to consider more complex geometries.

Appendix A. Notation Table

Symbol	Description	Symbol	Description
$0_{i,j}$	Zero matrix in $\mathbb{R}^{i\times j}$	0	Zero matrix of appropriate dimensions where there in no ambiguity
$I_{i,i}$	Identity matrix in $\mathbb{R}^{i\times i}$	$t > 0 \in \mathbb{R}$	time coordinate
$\xi,\ \xi_i \in \mathbb{R}$	1D and 2D spatial Cartesian coordinates, $i \in \{1,2\}$	$\alpha,\ \beta,\ \gamma \in \mathbb{R}$	2D spatial coordinates in the triangular case
$\frac{\partial \cdot}{\partial \xi}$	partial derivative with respect to ξ	$\frac{\delta \cdot}{\delta x}$	variational derivative with respect to function x
$\frac{\partial \cdot}{\partial t}$	partial derivative with respect to t	$L,\ L_i > 0 \in \mathbb{R}$	1D and 2D domain dimensions, $i \in \{1,2\}$
$q_1,\ q_2 > 0 \in \mathbb{R}$	constant physical parameters	$c_0 > 0 \in \mathbb{R}$	constant celerity of the wave
$L^2(\Omega, \mathbb{R}^n)$	space of square-integrable functions on the domain Ω with values in $\mathbb{R}^n$	$h > 0 \in \mathbb{R}$	spatial step in the 1D and triangular cases
$h_{\{1,2\}} > 0 \in \mathbb{R}$	spatial step in the 2D rectilinear case	$E_k,\ E_p$	kinetic energy, potential energy

To simplify the notation in the following of this appendix, define ($i \in \{1,2\},\ j \in \mathbb{N}$) in the 1D case, ($i \in \{1,2,3\},\ j \in \mathbb{N}^2$) in the 2D rectilinear case and ($i \in \{\alpha,\beta,\gamma,\varepsilon\},\ j \in \mathbb{N}$) in the 2D triangular case. The spatial domain Ω is equal to $[0, L]$ in the 1D case and to $[0, L_1] \times [0, L_2]$ in the 2D case.

Symbol	Description	Symbol	Description
$\mathcal{B}$	boundary of Ω	$\mathcal{X}$	space of energy variables, infinite dimensional case
$\mathcal{F}$	space of flows	$\mathcal{E}$	space of effort
$\mathcal{J} : \mathcal{E} \to \mathcal{F}$	skew-symmetric operator	$\mathcal{L} = \begin{pmatrix} \mu_0^{-1} & 0 \\ 0 & \chi_s^{-1} \end{pmatrix}$	energy matrix
$\mathcal{D} \subset \mathcal{F} \times \mathcal{E}$	Stokes Dirac structure	$\mathcal{H} : \mathcal{X} \to \mathbb{R}^+$	Hamiltonian, infinite dimensional case
$x_i,\ e_i,\ f_i$	state, effort and flow variables in infinite dimension	$x,\ e,\ f$	vectors of state, effort and flow in infinite dimension
$e_\partial,\ f_\partial$	infinite dimensional boundary variables	$x_j^i,\ e_j^i,\ f_j^i \in \mathbb{R}$	approximation at the point j of the state, effort and flow variables
$x_d^i,\ e_d^i,\ f_d^i \in \mathbb{R}^k$	approximation of the state, effort and flow variables, $k \in \mathbb{N}$	$x_d,\ e_d,\ f_d \in \mathbb{R}^k$	approximation of the vectors of states, efforts and flows, $k \in \mathbb{N}$
$e_{d\partial}^i,\ f_{d\partial}^i \in \mathbb{R}^k$	approximation of the boundary effort and flow variables, , $k \in \mathbb{N}$	$e_{d\partial}, f_{d\partial} \in \mathbb{R}^k$	approximation of the infinite dimensional vectors of boundary effort and flow, $k \in \mathbb{N}$
$J_d \in \mathbb{R}^{k\times k}$	skew-symmetric matrix, $k \in \mathbb{N}$	$L_d \in \mathbb{R}^{k\times k}$	positive definite diagonal matrix, $k \in \mathbb{N}$
$H_d : \mathbb{R}^k \to \mathbb{R} \geq 0$	Finite dimensional Hamiltonian, $k \in \mathbb{N}$	$\mathcal{D}_d \subset F \times E$	Dirac structure in finite dimension
$g_d \in \mathbb{R}^{k_1 \times k_2}$	input matrix, $\{k_1,\ k_2\} \in \mathbb{N}$	$u_c,\ y_c \in \mathbb{R}^k$	boundary controller input and output, $k \in \mathbb{N}$

$K_{\{1\ldots4\}}$, $K^{\partial}_{\{1\ldots5\}}$, D, $D_{\{1\ldots3\}}$, $D^{+}_{\{1\ldots3\}}$, $D^{-}_{\{1\ldots3\}}$, $g_{\{1,2\}}$ and $g_{\{\alpha\ldots\gamma\}}$ are real matrices introduced for the discretization of the differential operators and boundary inputs. Integers are defined to number the discrete points:

Symbol	Description	Symbol	Description
$n \in \mathbb{N}$	number of points where x_2 is defined, 1D case	$m,\ n \in \mathbb{N}$	number of lines and columns where x_2 is defined, rectilinear case
$n_{tl},\ n_{tc} \in \mathbb{N}$	number of triangles per line and per column, triangular case	$n_i \in \mathbb{N}$	number of points where x_i is defined, triangular case
$n^{\partial}_i \in \mathbb{N}$	number of boundary points where x_i is defined, triangular case	$n_d \in \mathbb{N}$	total number of discrete points, triangular case
$n^{\partial}_d \in \mathbb{N}$	total number of boundary discrete points, triangular case	$m,\ n,\ o \in \mathbb{N}$	numbering of the coordinates over the three axes, triangular case

Appendix B. Time Integration

This appendix details the time integration methods of the discretized wave equation exploited Section 4. There are no original contributions in this appendix. It aims at completing the spatial discretization with time integration for the paper to be self-contained.

B.1. Implicit midpoint

The implicit midpoint method is the simplest symplectic method of order 2 [34]. Consider an ordinary differential equation such as $\dot{x} = g(x)$ where the state $x \in \mathbb{R}^n$, $n \in \mathbb{N}$. Applying the implicit midpoint scheme for a chosen step time $\delta_t \in \mathbb{R}^+$ with $x_k \approx x(k\delta_t)$ leads to the following scheme:

$$x_{k+1} = x_k + \delta_t g\left(\tfrac{x_k + x_{k+1}}{2}\right).$$

When applied to the conservative discretized port-Hamiltonian system (15), this scheme becomes

$$x_{k+1} = \left(I - \tfrac{\delta t}{2} J_d L_d\right)^{-1} \left(x_k + \tfrac{\delta t}{2}\left(J_d L_d x_k + g_d(u_k + u_{k+1})\right)\right)$$

when $\left(I - \frac{\delta t}{2} J_d L_d\right)$ is invertible, which may depend of the chosen δ_t.

The midpoint method can be applied to dissipative port-Hamiltonian systems [2] by replacing J_d by $(J_d - R_d)$ in the previous equation, with R_d the dissipation matrix of the discrete system, symmetric positive definite.

In the linear case, this method coincides with the discrete gradient method, which respects the power balance of the system [36,47]. In the conservative case, this property guaranties that the discrete Hamiltonian remains constant along the time integration.

B.2. Störmer–Verlet

The Störmer–Verlet method, also called leap-frog method, is an integration method for separable Hamiltonian systems. It is the most widely used method for computations in molecular dynamics [35]. Like the midpoint method, it is a symplectic method of order 2, and is thus particularly suited to consider conservative systems.

Consider the discretized 1D wave equation (15) with this two steps integration method implies to express separately the discrete approximations of the conservation laws which underlie the wave equation:

$$\begin{aligned}\dot{x}^1_d &= D\chi_s^{-1} x^2_d + g_a u_d \\ \dot{x}^2_d &= -D^\top \mu_0^{-1} x^1_d + g_b u_d\end{aligned}$$

where g_a and g_b are composed of the appropriate number of first and last rows of g_d, respectively. For a chosen step time $\delta_t \in \mathbb{R}^+$ with $x^i_k \approx x^i_d(k\delta_t)$, $i \in \{1, 2\}$, the integration scheme is

$$\begin{aligned}x^1_{k+0.5} &= x^1_k + \tfrac{\delta t}{2}\left(-D\chi_s^{-1} x^2_k + g_a u_k\right) \\ x^2_{k+1} &= x^2_k + \delta t\left(D^\top \mu_0^{-1} x^1_{k+0.5} + g_b u_{k+1}\right) \\ x^1_{k+1} &= x^1_{k+0.5} + \tfrac{\delta t}{2}\left(-D\chi_s^{-1} x^2_{k+1} + g_a u_{k+1}\right).\end{aligned}$$

Or, equivalently

$$\begin{aligned} x^2_{k+0.5} &= x^2_k + \tfrac{\delta t}{2}\left(D^\top \mu_0^{-1} x^1_k + g_b u_k\right) \\ x^1_{k+1} &= x^1_k + \delta t\left(-D\chi_s^{-1} x^2_{k+0.5} + g_a u_{k+1}\right) \\ x^2_{k+1} &= x^2_{k+0.5} + \tfrac{\delta t}{2}\left(D^\top \mu_0^{-1} x^1_{k+1} + g_b u_{k+1}\right). \end{aligned}$$

One notices that this scheme does not permit to take into account internal dissipation trivially.

References

[1] A. van der Schaft, L2-Gain and Passivity Techniques in Nonlinear Control, 3rd edition, Springer-Verlag, 2017.
[2] V. Duindam, A. Macchelli, S. Stramigioli, H. Bruyninckx (Eds.), Modeling and Control of Complex Physical Systems – The Port-Hamiltonian Approach, Springer, 2009.
[3] B. Maschke, A. van der Schaft, Port controlled Hamiltonian systems: modeling origins and system theoretic properties, in: Proceedings of the 3rd IFAC Symposium on Nonlinear Control Systems, NOLCOS'92, Bordeaux, France, 1992, pp. 282–288.
[4] R. Ortega, A. van der Schaft, B. Maschke, G. Escobar, Interconnection and damping assignment passivity based control of port-controlled Hamiltonian systems, Automatica 38 (2002) 585–596.
[5] A. van der Schaft, B. Maschke, Hamiltonian formulation of distributed-parameter systems with boundary energy flow, J. Geom. Phys. 42 (1–2) (2002) 166–194.
[6] Y. Le Gorrec, H. Zwart, B. Maschke, Dirac structures and boundary control systems associated with skew-symmetric differential operators, SIAM J. Control Optim. 44 (5) (2005) 1864–1892.
[7] J. Villegas, H. Zwart, Y. Le Gorrec, B. Maschke, Exponential stability of a class of boundary control systems, IEEE Trans. Autom. Control 54 (2009) 142–147.
[8] B. Jacob, H. Zwart, Linear Port-Hamiltonian Systems on Infinite-dimensional Spaces, Oper. Theory, Adv. Appl., vol. 223, Birkhäuser, Basel, Switzerland, 2012.
[9] H. Ramirez, Y. Le Gorrec, A. Macchelli, H. Zwart, Exponential stabilization of boundary controlled port-Hamiltonian systems with dynamic feedback, IEEE Trans. Autom. Control 59 (10) (2014) 2849–2855.
[10] A. Macchelli, Y.L. Gorrec, H. Ramirez, H. Zwart, On the synthesis of boundary control laws for distributed port Hamiltonian systems, IEEE Trans. Autom. Control 62 (4) (2016) 1700–1713.
[11] M. Seslija, A. van der Schaft, J.M. Scherpen, Discrete exterior geometry approach to structure-preserving discretization of distributed-parameter port-Hamiltonian systems, J. Geom. Phys. 62 (6) (2012) 1509–1531.
[12] G. Golo, V. Talasila, A. van der Schaft, B. Maschke, Hamiltonian discretization of boundary control systems, Automatica 40 (5) (2004) 757–771.
[13] B. Hamroun, L. Lefevre, E. Mendes, Port-based modelling and geometric reduction for open channel irrigation systems, in: 46th IEEE Conference on Decision and Control, IEEE, 2007, pp. 1578–1583.
[14] R. Moulla, L. Lefévre, B. Maschke, Pseudo-spectral methods for the spatial symplectic reduction of open systems of conservation laws, J. Comput. Phys. 231 (4) (2012) 1272–1292.
[15] P. Kotyczka, B. Maschke, Discrete port-Hamiltonian formulation and numerical approximation for systems of two conservation laws, Automatisierungstechnik 65 (5) (2017) 308–322.
[16] L. Bassi, A. Macchelli, C. Melchiorri, An algorithm to discretize one-dimensional distributed port Hamiltonian systems, in: Lagrangian and Hamiltonian Methods for Nonlinear Control 2006, Springer, 2007, pp. 61–73.
[17] A. Macchelli, Energy shaping of distributed parameter port-Hamiltonian systems based on finite element approximation, Syst. Control Lett. 60 (8) (2011) 579–589.
[18] Y. Wu, B. Hamroun, Y. Le Gorrec, B. Maschke, Power preserving model reduction of 2D vibro-acoustic system: a port Hamiltonian approach, in: Conference on Lagrangian and Hamiltonian Methods for Non-Linear Control, LHMNLC'15, Lyon, France, 2015, pp. 206–211.
[19] Y. Le Gorrec, H. Peng, L. Lefèvre, B. Hamroun, F. Couenne, Systèmes hamiltoniens à ports de dimension infinie: réduction et propriétés spectrales, J. Eur. Syst. Autom. 45 (7–10) (2011) 645–664.
[20] P. Kotyczka, Finite volume structure-preserving discretization of 1D distributed-parameter port-Hamiltonian systems, in: Proc. 2nd IFAC Workshop on Control of Systems Governed by Partial Differential Equations, Bertinoro, Italy, 2016, pp. 300–305.
[21] P. Kotyczka, B. Maschke, L. Lefèvre, Weak form of Stokes–Dirac structures and geometric discretization of port-Hamiltonian systems, J. Comput. Phys. 361 (2018) 442–476.
[22] S. Mazumder, Numerical methods for partial differential equations, in: Finite Difference and Finite Volume Methods, Elsevier, 2015.
[23] J.C. Strikwerda, Finite Difference Schemes and Partial Differential Equations, Siam, 2004.
[24] A. Iserles, Generalized leapfrog methods, IMA J. Numer. Anal. 6 (4) (1986) 381–392.
[25] B. Fornberg, High-order finite differences and the pseudospectral method on staggered grids, SIAM J. Numer. Anal. 27 (4) (1990) 904–918.
[26] Y.Q. Zeng, Q.H. Liu, A staggered-grid finite-difference method with perfectly matched layers for poroelastic wave equations, J. Acoust. Soc. Am. 109 (6) (2001) 2571–2580.
[27] B. Hustedt, S. Operto, J. Virieux, Mixed-grid and staggered-grid finite-difference methods for frequency-domain acoustic wave modelling, Geophys. J. Int. 157 (3) (2004) 1269–1296.
[28] I. Štekl, R.G. Pratt, Accurate viscoelastic modeling by frequency-domain finite differences using rotated operators, Geophysics 63 (5) (1998) 1779–1794.
[29] C. Shin, H. Sohn, A frequency-space 2-d scalar wave extrapolator using extended 25-point finite-difference operator, Geophysics 63 (1) (1998) 289–296.
[30] R.W. Graves, Simulating seismic wave propagation in 3d elastic media using staggered-grid finite differences, Bull. Seismol. Soc. Am. 86 (4) (1996) 1091–1106.
[31] B. Hamilton, S. Bilbao, Hexagonal vs. rectilinear grids for explicit finite difference schemes for the two-dimensional wave equation, in: Proceedings of Meetings on Acoustics, vol. 19, Acoustical Society of America, 2013, p. 015120.
[32] S. Bilbao, Modeling of complex geometries and boundary conditions in finite difference/finite volume time domain room acoustics simulation, IEEE Trans. Audio Speech Lang. Process. 21 (7) (2013) 1524–1533.
[33] D.W. Zingg, H. Lomax, Finite-difference schemes on regular triangular grids, J. Comput. Phys. 108 (2) (1993) 306–313.
[34] L.V. Kantorovich, Approximate Methods of Higher Analysis, Noordhoff, 1958.
[35] E. Hairer, C. Lubich, G. Wanner, Geometric Numerical Integration: Structure-Preserving Algorithms for Ordinary Differential Equations, vol. 31, Springer Science & Business Media, 2006.

[36] D.S. Laila, A. Astolfi, Construction of discrete-time models for port-controlled hamiltonian systems with applications, Syst. Control Lett. 55 (8) (2006) 673–680.
[37] A. Falaize, T. Hélie, Passive simulation of the nonlinear port-Hamiltonian modeling of a Rhodes piano, J. Sound Vib. 390 (2017) 289–309.
[38] V. Trenchant, H. Ramirez, Y. Le Gorrec, P. Kotyczka, Structure preserving spatial discretization of 2D hyperbolic systems using staggered grids finite difference, in: American Control Conference (ACC), IEEE, 2017, pp. 2491–2496.
[39] M. Collet, M. Ouisse, M. Ichchou, R. Ohayon, Semi-active optimization of 2D wave's dispersion into shunted piezocomposite systems for controlling acoustic interaction, in: ASME 2011 Conference on Smart Materials, Adaptive Structures and Intelligent Systems, American Society of Mechanical Engineers, 2011, pp. 79–87.
[40] M. Collet, P. David, M. Berthillier, Active acoustical impedance using distributed electrodynamical transducers, J. Acoust. Soc. Am. 125 (2) (2009) 882–894.
[41] V. Trenchant, Y. Fares, H. Ramirez Estay, Y. Le Gorrec, M. Ouisse, A port-Hamiltonian formulation of a 2D boundary controlled acoustic system, in: Conference on Lagrangian and Hamiltonian Methods for Non-Linear Control, LHMNLC'15, Lyon, France, 2015, pp. 1–8.
[42] N.W. Hagood, A. von Flotow, Damping of structural vibrations with piezoelectric materials and passive electrical networks, J. Sound Vib. 146 (2) (1991) 243–268.
[43] C. Hansen, S. Snyder, X. Qiu, L. Brooks, D. Moreau, Active Control of Noise and Vibration, CRC Press, 2012.
[44] W. Thiel, L.P. Katehi, Some aspects of stability and numerical dissipation of the finite-difference time-domain (fdtd) technique including passive and active lumped elements, IEEE Trans. Microw. Theory Tech. 50 (9) (2002) 2159–2165.
[45] H. Nijmeijer, A. van der Schaft, Nonlinear Dynamical Control Systems, Springer-Verlag, New York, USA, 1990.
[46] B. Hamilton, A. Torin, Finite Difference Schemes on Hexagonal Grids for Thin Linear Plates with Finite Volume Boundaries, DAFx, Citeseer, 2014, pp. 5–12.
[47] A. Falaize, Modélisation, simulation, génération de code et correction de systèmes multi-physiques audios: approche par réseau de composants et formulation hamiltonienne à ports, Ph.D. thesis, Université Pierre & Marie Curie, Paris 6, 2016.
[48] M. Krstic, A. Smyshlyaev, Boundary Control of PDEs: A Course on Backstepping Designs, vol. 16, Siam, 2008.
[49] B. Brogliato, R. Lozano, B. Maschke, O. Egeland, Dissipative Systems Analysis and Control, 2nd edition, Comm. Control Engrg. Ser., Springer-Verlag, London, 2007.